Reviews in Mineralogy & Geochemistry
Vol. 80 pp. 355-391, 2015

Isotopic Gradients Across Fluid–Mineral Boundaries

Jennifer L. Druhan

Department of Geology
University of Illinois at Urbana-Champaign
Urbana, Illionois 61801, USA
and
Department of Geological and Environmental Sciences
Stanford University
Stanford, California 94305, USA

jdruhan@illinois.edu

Shaun T. Brown

Earth Sciences Division
Lawrence Berkeley National Laboratory
Berkeley, California 94720, USA
and
Department of Earth and Planetary Science
University of California Berkeley
Berkeley, California 94720, USA

stbrown@lbl.gov

Christian Huber

School of Earth and Atmospheric Sciences
Georgia Institute of Technology
Atlanta, Georgia 30332, USA

christian.huber@eas.gatech.edu

INTRODUCTION

The distribution of stable and radiogenic isotopes within and among phases provides a critical means of quantifying the origin, residence and cycling of materials through terrestrial reservoirs (Wahl and Urey 1935; Epstein and Mayeda 1953; Johnson et al. 2004; Eiler 2007; Porcelli and Baskaran 2011; Wiederhold 2015). While isotopic variability is globally observable, the mechanisms that govern both their range and distribution occur largely at atomic (e.g., radioactive decay), molecular (e.g., the influence of mass on the free energy of atomic bonds) and pore (e.g., diffusive transport to reactive surface) scales. In contrast, the vast majority of isotope ratio measurements are based on sample sizes that aggregate multiple pathways, species and compositions. Inferring process from such macro-scale observations therefore requires unraveling the relative contribution of a variety of potential mechanisms. In effect, the use of isotopes as proxies to infer a specific parameter, such as temperature (Urey 1947) or residence time (Kaufman and Libby 1954), carries the implicit requirement that one mechanism is the primary influence on the measured isotopic composition of the composite sample.

1529-6466/15/0080-0011$05.00 http://dx.doi.org/10.2138/rmg.2015.80.11

In the present chapter, we consider a wide variety of macro-scale observations of isotope partitioning across fluid–solid phase boundaries. For this purpose we define the continuum scale as a representation in which interfaces are averaged over elementary volumes, as opposed to the pore scale in which these interfaces are explicitly resolved. Throughout this review it will be demonstrated that observations of isotope partitioning across fluid–solid boundaries require some representation of the isotopic composition of the solid surface and surrounding fluid distinct from 'bulk' or 'well mixed' reservoirs. For example, this distinction is necessary in order to (1) quantify the partitioning of radioactive and radiogenic species, (2) describe transport limitations that may impact the macroscopic partitioning of isotope ratios, (3) explain observations of transient fractionation due to dissolution through preferential release at the solid surface, and (4) parameterize apparently variable fractionation factors during precipitation. The ability to describe isotopic partitioning specific to the phase boundary then influences the accuracy of simulations from highly variable, field scale systems (e.g., Druhan et al. 2013) to highly controlled laboratory experiments (e.g., Tang et al. (2008)). ***These observations imply that quantifying the composition of solids and fluids as averages across a given representative volume carries some inherent loss of information that isotopes appear to be sensitive to***. This conclusion leads us to consider mechanistic descriptions of isotope partitioning that could be significantly improved by modeling approaches that are capable of resolving spatial zoning within individual solids (e.g., Li et al. 2006; Tartakovsky et al. 2008; Molins et al. 2012; Molins 2015, this volume; Yoon et al. 2015, this volume).

The suite of experimental data and quantitative approaches described herein support a conceptual framework in which macroscopic observables, such as an apparent fractionation factor, are the emergent result of multiple interacting processes that are strongly influenced by the physical and chemical characteristics of the fluid–solid boundary. In this sense we consider the pore scale as a characteristic length over which the unique physical and chemical properties of the phase interface may be described as distinct from bulk or aggregate values. This definition of the pore scale provides a critical reference frame over which molecular scale mechanisms combine to yield the macroscopic observables (Steefel et al. 2013).

A conceptual model of isotope partitioning at the pore scale

The flux of solutes in porous media is influenced by the development of spatial and temporal gradients resulting from the combined effects of transport and reactivity. How the pore-scale nature of these processes emerges into continuum scale observations of fluid–solid interaction is yet unresolved and requires multiscale (e.g., fractal) upscaling methods that remain a challenge. For example, Darcy scale fluid flow may occur along a fixed gradient, but the size, shape and distribution of individual solid grains is such that at the pore scale velocity vectors vary in both magnitude and direction. As a result, the principle mechanism of solute transport in some areas is advective, while in others it is diffusive. Mixing between these distinct regimes is approximated at the continuum scale by either a heterogeneous conductivity field (Li et al. 2010; Sudicky et al. 2010), a hydrodynamic dispersion coefficient (Gelhar and Axness 1983; Steefel and Maher 2009) or a non-uniform fluid travel time distribution (Maloszewski and Zuber 1982; Bellin and Tonina 2007).

Reactions that occur between fluid and solid phases are influenced by these local pore-scale transport regimes. For example, where transport of solutes between a solid surface and a surrounding fluid is accomplished primarily by diffusion, the rate of reaction across that interface may be limited by either the delivery of solute to the reactive surface or the approach to equilibrium. When advection is dominant, the same process may be governed by the relative rates of reactivity and flow (Rolle et al. 2009; Maher 2010; Hochstetler et al. 2013). The factors influencing isotopic partitioning are then equally variable across the pore scale (Fig. 1). In areas of the domain governed by diffusion, the partitioning of isotopes may reflect a transport limitation or diffusive fractionation, whereas in areas where flow is relatively fast, the isotopic

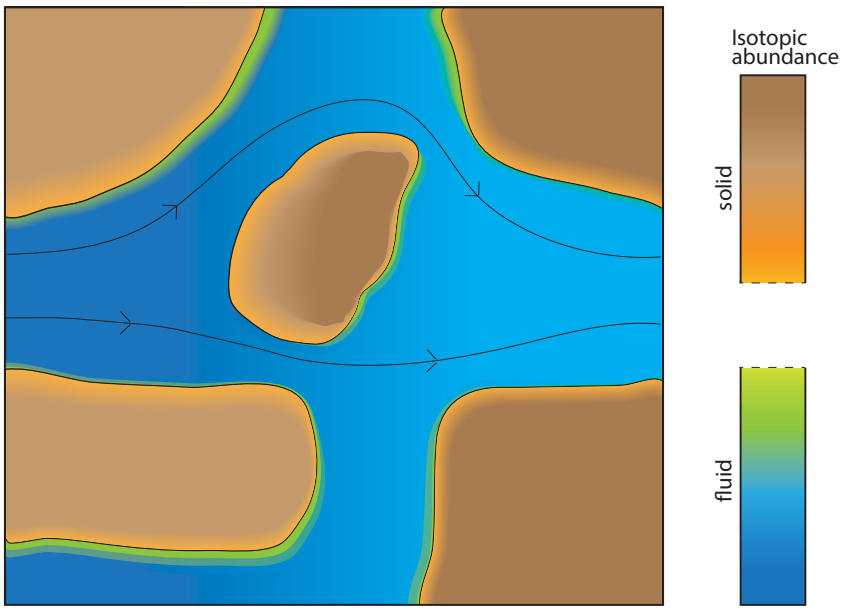

Figure 1. Conceptual model of isotopic partitioning at the pore scale during fluid–rock interaction. Darcy-scale flow occurs from left to right, whereas at the pore scale local variations in both magnitude and direction lead to areas of the domain that are either advection or diffusion dominated. The bulk fluid isotopic composition also varies from left to right as a result of reaction progress, but the isotopic composition of fluid and the solid surface is subject to multiple fractionating processes and thus variable. The precipitation of new solid or dissolution of existing solid is then also isotopically variable and distinct from the bulk.

composition is likely governed by the partitioning associated with a reaction (Lemarchand et al. 2004; Fantle and DePaolo 2007; DePaolo 2011). The accumulation of newly formed solids is also anticipated to vary with the local transport regime, which in turn exerts an influence on the isotopic composition of the fluid–solid interface.

This relationship between the dominant mechanisms of transport and fractionation suggests that over a representative volume of porous media a variety of fractionation factors may be observed. For example a fractionation factor characteristic of diffusive transport between the solid–fluid surface and the well-mixed fluid, or a fractionation factor associated with the difference in isotope composition between the fluid and solid at each reactive surface. The continuum-scale or observable fractionation factor over the timescale of the reaction (e.g., seconds to years) is then subject to the location and volume of material sampled. Over much longer periods of time, processes like recrystallization and solid-state diffusion homogenize spatial zoning within the solid. This implies that transient isotopic partitioning should be observable over significant periods of time, and that the observed macroscopic fractionation factor is potentially (1) a combination of multiple, distinct mechanisms and (2) variable as a result of parameters such as saturation state and flow rate.

From this perspective, variability in the magnitude of an observed fractionation factor is in some ways analogous to the discrepancy in rate constants observed across natural systems (Malmstrom et al. 2000; White and Brantley 2003; Maher et al. 2006b). This wide range in what should in principle be a fixed value has been attributed to the relative influence of a variety of processes, such as changes in reactive surface area (VanCappellen 1996), transport limitation (Steefel and Lichtner 1998; Maher 2011; Li et al. 2014); and even climate variations (Kump et al. 2000; Maher and Chamberlain 2014). Similarly, the apparent isotopic partitioning observed in flux-weighted or homogenized natural samples is often distinct from that obtained under controlled experimental conditions. These effects have been noted in a

variety of contexts, including oxygen and nitrogen isotope fractionation in marine sediments (Brandes and Devol 1997), selenium isotope fractionation in wetlands (Clark and Johnson 2008), compound-specific stable isotope analysis (CSIA) of organics (Van Breukelen 2007) and chromium isotope fractionation in a contaminated aquifer (Berna et al. 2010).

To the extent that pore structure influences the distribution of isotope ratios in reactive systems, using volume-averaged sample measurements to quantify related parameters, such as reaction progress or mixing, can result in significant uncertainty. For example, both analytical and numerical solutions have demonstrated that neglecting the effects of hydrodynamic dispersion on observed stable isotope ratios can lead to an underestimation of reactivity in through-flowing systems (Abe and Hunkeler 2006; Van Breukelen and Prommer 2008). As noted above, dispersion is one method of parameterizing mixing at the continuum scale, and thus approximating the contribution of distinct fluid isotopic compositions at the pore scale (Fig. 1). Improved accuracy should then be achievable by describing distributed pore-scale isotopic compositions as the result of a variety of mechanisms, e.g., multiple fractionating reactions, a difference in the diffusion coefficient of the isotopologues of a compound or the dampening of a kinetic fractionation as a result of transport limitation. In the current article, we consider observations of isotopic partitioning across fluid–solid boundaries associated with a variety of fractionating mechanisms. In reviewing these examples we emphasize the aspects of each process that lead to pore-scale heterogeneity and thus a disconnect in behavior between the scale of mechanism and the scale of observation. These categories are by no means an exhaustive list of all processes that result in isotopic partitioning across reactive interfaces, but serve as examples in which interpreting the response of continuum-scale isotopic values to variations in external parameters is improved by consideration of pore-scale isotopic distributions.

Organization of article

The structure of the article is broadly divided into three sections. First, we provide a brief explanation of the notation used to describe isotope partitioning, with an accompanying discussion of primary mechanisms and models for fractionation. Second, we describe experimental observations for four examples of isotopic partitioning across fluid–mineral interfaces: α-recoil, diffusion, dissolution, and precipitation. Across this wide range of processes, a common observation is that the interface between fluid and solid phases (1) governs material transfer between reservoirs and (2) displays isotopic compositions distinct from bulk values. Associated models for the mass balance at phase boundaries are described with particular emphasis on the mechanisms necessary in order to quantify macroscale observations. This leads to the second section in which current modeling techniques for the description of transient isotopic final and the development of zoned mineral grains are discussed, concluding with a novel application of pore-scale modeling techniques to describe the distribution of stable isotopes across a fluid–mineral boundary as an initially oversaturated system establishes equilibrium. Throughout this review the principal intent is to describe experimental and modeling studies of isotopic partitioning with reference to the ways in which the composition and gradients across fluid–mineral boundaries is distinct from bulk-averaged values and uniquely influences continuum-scale observations.

NOTATION

The exchange of material across fluid–mineral surfaces influences both radiogenic and stable isotope distributions. Unlike (most) stable isotope fractionation, variations in radiogenic isotopes are mass-independent and arise due to the radioactive decay of a parent nuclide to an intermediate radioactive nuclide or a stable, radiogenic nuclide. The uranium decay series (Fig. 2) illustrates the relationship amongst parent and daughter isotopes, and the terminology is applicable to other radioactive-radiogenic systems.

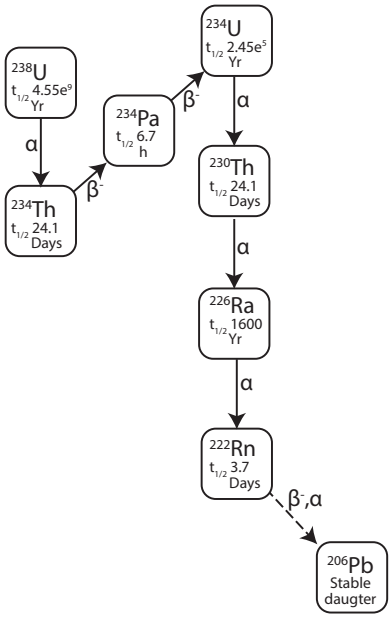

Figure 2. Simplified illustration of the ^{238}U decay series. The half-life and primary decay path are indicated for each isotope.

The ^{238}U isotope is radioactive and for N nuclei at time t in a closed system the number of decaying nuclei dN in the time interval dt follows a homogeneous Poisson statistical law and is proportional to N:

$$\lambda = -\frac{1}{N}\frac{\mathrm{d}n}{\mathrm{d}t} \tag{1}$$

where lambda (λ) is the decay constant. The expression on the right side is a probability per unit time of a radioactive decay event. Integration of Equation (1) yields an exponential equation for radioactive decay:

$$N(t) = N_0 e^{-\lambda t} \tag{2}$$

where the integration constant (N_0) is equal to the initial number of nuclei at $t = 0$. The decay constant is related to the nuclide half-life

$$t_{1/2} = \frac{\ln(2)}{\lambda} \tag{3}$$

For intermediate daughter products such as ^{234}U and ^{226}Ra, isotopic abundance is commonly discussed in terms of activity (A) where:

$$A(t) = \lambda N(t) \tag{4}$$

and thus the initial activity at $t = 0$ is $A_0 = \lambda N_0$. In a closed system that starts with no daughter isotopes, for example the ^{238}U- ^{234}U system, the initial activity of ^{234}U is zero and it will increase until $A_{238_U} = A_{234_U}$. At this point the supply of ^{234}U from ^{238}U decay is balanced by the decay of ^{234}U to ^{230}Th, representing a steady state where the ratio of λ limits the maximum possible intermediate daughter activity. When $A_1 = A_2$ this is a special condition

known as secular equilibrium. In the remainder of the chapter we will use the notation $^{234}\mathrm{U}/^{238}\mathrm{U}_{\mathrm{AR}} = A_{234_{\mathrm{U}}} / A_{238_{\mathrm{U}}}$ where the subscript AR denotes the activity ratio.

Finally, for stable radiogenic daughter isotopes (e.g., ^{206}Pb, in the ^{238}U series), accumulation of isotope N_2 is related to the initial abundance of the parent isotope (N_0) and time:

$$N_2 = N_0\left(1 - e^{-\lambda_1 t}\right) \tag{5}$$

such that as t goes to infinity N_2 goes to N_0. Krane (1988) presents an exhaustive discussion of radioactive decay including considerations for branched decay, and very short-lived intermediate daughter isotopes. The subsequent discussion will use the ^{238}U–^{234}U system to consider the influence of pore-scale effects in quantifying α-recoil damage and associated alterations to solid surfaces and solution chemistry.

As noted above, there can be ambiguity in the notation used to describe the partitioning of stable isotopes. In the subsequent text we primarily adhere to the guidelines put forth by Coplen (2011). The isotope ratio (R) of a particular reservoir is defined as

$$R\left({}^{i}E / {}^{j}E\right)_P = N({}^{i}E)_P / N\left({}^{j}E\right)_P \tag{6}$$

where N is the number of atoms of ${}^{i}E$ and ${}^{j}E$, the isotopes i and j of the element E in substance P. This value is commonly reported relative that of a standard ratio (std), referred to as the delta value (δ), and defined as

$$\begin{aligned} \delta^{i}E_P &= \left(R\left({}^{i}E / {}^{j}E\right)_P - R\left({}^{i}E / {}^{j}E\right)_{\mathrm{std}}\right) / R\left({}^{i}E / {}^{j}E\right)_{\mathrm{std}} \\ &= R\left({}^{i}E / {}^{j}E\right)_P / R\left({}^{i}E / {}^{j}E\right)_{\mathrm{std}} - 1 \end{aligned} \tag{7}$$

This delta value is nondimensional, but is commonly multiplied by 1000 to report values as parts per thousand or per mil (‰). The difference between the isotope ratios (Δ) of two compounds or phases (P and Q) is then

$$\Delta^{i}E_{P/Q} = \delta^{i}E_P - \delta^{i}E_Q \tag{8}$$

The apparent or net isotopic fractionation factor does not make use of delta notation, but is defined as

$$\alpha^{i}E_{P/Q} = R\left({}^{i}E / {}^{j}E\right)_P / R\left({}^{i}E / {}^{j}E\right)_Q \tag{9}$$

Conversion between $\Delta^{i}E_{P/Q}$ and $\alpha^{i}E_{P/Q}$ may be approximated as $\Delta^{i}E_{P/Q} \approx \ln \alpha^{i}E_{P/Q}$. From these relationships it is noted that both the difference between the isotope ratios (Eqn. 8) and the apparent fractionation factor (Eqn. 9) between two reservoirs are obtained from direct measurement regardless of the variety of reaction pathways necessary to produce them, and are therefore a function of the representative volume of the sample in all but the most simplified systems. In contrast, a fractionation factor associated with a specific reaction pathway may be derived in reference to the rate law for that reaction. These types of fractionating processes are discussed in the subsequent section. Finally, an isotopic mole fraction (X) may be defined as the ratio of the amount of a particular isotope in a given species, compound, or reservoir divided by the total amount of that element in the same group

$$X^{i}E_P = n\left({}^{i}E\right)_P / \sum n\left(E\right) \tag{10}$$

This value is used in the derivation of isotope-specific reversible rate expressions that involve a solid phase.

A note on fractionation

In this chapter, stable isotope fractionation will be discussed in terms of equilibrium and kinetic processes. For this purpose chemical equilibrium is described as a dynamic state that occurs when two elementary reactions, the forward reaction from reactants to products and the backward reaction from products to reactants, are in balance. For example, the hydroxylation of dissolved CO_2:

$$CO_2 + OH^- \Leftrightarrow HCO_3^- \tag{11}$$

which is at equilibrium when in a closed system the distribution of species is invariant in time. The ratio of the elementary forward and backward rates is then termed the equilibrium constant (K_{eq}). Isotopic equilibrium may be described similarly, for example considering carbon isotope equilibrium between the carbon-bearing species in Equation (11):

$$^{12}CO_2 + H^{13}CO_3^- \Leftrightarrow {}^{13}CO_2 + H^{12}CO_3^- \tag{12}$$

leading to a separate equilibrium constant to account for this isotopic partitioning. A comparable relationship could be written for the partitioning of oxygen isotopes between CO_2 and HCO_3^-, or between HCO_3^- and OH^-. While all of these equilibria are described using the same law of mass action, it is important to note that they are not predicated on one another. In other words, these descriptions allow for the establishment of chemical equilibrium without necessarily requiring isotopic equilibrium. For reactions involving simple stoichiometric relationships, where one atom of the element of interest occurs in all reactant and product species, the isotopic equilibrium constant is equivalent to the fractionation factor (Eqn. 9); however, the relationship is often more complex (Schauble 2004). In general, the equilibrium fractionation factor is temperature dependent and larger for low mass elements and for isotopes of the same element that have large differences in mass. Typically, the partitioning of stable isotopes between two phases at equilibrium preferentially incorporates the heavier isotope in the phase with lower bond energy.

An imbalance between the forward and backward rates leads to a net accumulation of either the product or reactant, and the rate of this mass transfer is described by kinetics. Many reactions take place under conditions in which the reverse reaction is in some way prohibited, or the system is very far from equilibrium, such that isotopic partitioning is entirely kinetic. A kinetic fractionation factor is expressed as the ratio of the isotopic composition of the instantaneously generated product species (P_{inst}) and the residual reactant (Q) through a single reaction pathway:

$$\alpha_{kin}\, {}^{i}E_{P/Q} = R\left({}^{i}E / {}^{j}E\right)_{P_{inst}} / R\left({}^{i}E / {}^{j}E\right)_{Q} \tag{13}$$

This α_{kin} can be related to the kinetic rate constant of the reaction (k), depending on the order of the reaction. For example, a first order dependence on concentration (e.g., $dP/dt = kQ$), leads to an expression for $\alpha_{kin} = {}^{i}k/{}^{j}k$ (Mariotti et al. 1981). From an observational perspective it is often difficult to categorically identify equilibrium vs. kinetic effects on isotope partitioning. In low-temperature systems equilibration can be extremely slow, and, in addition, open system conditions may support the establishment of a steady state that appears balanced but is not necessarily equilibrated. In this sense the distinction between a specific state that is dynamic equilibrium, and an observable net rate of precipitation or dissolution does not imply an exclusive influence of equilibrium vs. kinetic fractionation. The approach towards an equilibrated system implies instead a continuum between pure kinetic fractionation and equilibrium fractionation. Later sections of this chapter explore the consequences of such a model and the extent to which pore scale treatments are capable of improving upon current approaches.

Under certain conditions, it is possible to develop theoretical models to predict the evolution of the isotopic composition of products and reactants. These models offer the advantage that they are simple to use, but are generally limited by particular assumptions and do not reflect the complexity of the reaction pathway or the relationship between transport and reaction in the isotopic mass balance description. Rayleigh fractionation, for instance, assumes an open system distillation process, where the reactant is progressively consumed, such that the isotope ratio of the reactant follows (Rayleigh 1902):

$$R = R_0 f^{(\alpha-1)} \tag{14}$$

where the isotope ratio (Eqn. 6) is equal to the product of the initial isotope ratio (R_0) and the fraction of reactant remaining relative to the initial concentration (f) raised to the power ($\alpha-1$). This relationship requires a constant fractionation factor α, and produces an exponential relationship between reaction progress and isotopic partitioning. This model is only strictly intended for systems in which the reactant is continually supplied (f cannot go to zero) and the product of the reaction is instantaneously removed or segregated from the reactive system (Criss 1999). In practice the Rayleigh model is used in a wide variety of systems because it offers a simple relationship between reaction progress and fractionation without requiring knowledge of the reaction pathway or transport mechanisms. As a result, several studies have pointed out limitations to the Rayleigh model in application to hydrogeochemical systems (Brandes and Devol 1997; Abe and Hunkeler 2006; Van Breukelen and Prommer 2008). A goal of the current chapter is to describe a variety of common fractionating mechanisms that often undermine the assumptions of such simplified models and promote new quantitative methods for explicit treatment of reactivity and transport in the description of isotope partitioning.

EXAMPLES OF ISOTOPIC ZONING ACROSS FLUID–SOLID BOUNDARIES

Alpha recoil

Prior to the development of modern radioactive decay counting and mass spectrometry techniques it was widely assumed that the $^{234}U/^{238}U_{AR}$ could not deviate from secular equilibrium. This was assumed to be the case because the small mass difference (~1.7%) of the two isotopes would not produce stable isotope effects like those observed for hydrogen and oxygen. Careful study of natural rocks and minerals in the 1950's, however, revealed variations from secular equilibrium (Chalov 1959). Since the chemical behavior of ^{234}U and ^{238}U should be nearly identical, and yet variations in $^{234}U/^{238}U_{AR}$ can exceed 500%, researchers suggested that the energy associated with ^{238}U decay could directly eject the ^{234}Th daughter isotope from the mineral surface (10's of nm) or damage the mineral lattice allowing preferential leaching of the daughter isotope (Rosholt et al. 1963; Kigoshi 1971).

Kigoshi (1971) carried out a pioneering study where fine-grained zircon sand was suspended in dilute aqueous solutions and the addition of ^{234}Th and ^{234}U to the solution was quantified. The ^{234}Th activities of the solutions were consistent with predicted α-recoil injection to the solution based upon a spherical grain model and an α-recoil distance of 55 nm. Earlier inferences (Turkowsky 1969) and later laboratory studies (Fleischer 1988) suggest that the recoil distance is closer to 30–40 nm. Both the ^{234}Th and ^{234}U in the fluid increased with time at a rate greater than the increase in ^{238}U, demonstrating that ^{234}Th has a recoil distance of tens of nm and can be ejected from the mineral structure or preferentially leached from lattice defects (Kigoshi 1971; Fleischer and Raabe 1978).

Kigoshi (1971) calculated the expected rate of addition of ^{234}Th to a fluid (Q) due to α-recoil ejection from a mineral grain based on:

$$Q = \frac{1}{4} LSN_{238}\,\rho\lambda_{238} \tag{15}$$

where L is the α-recoil range, S is the surface area, ρ is the solid density, and N_{238} and λ_{238} are the number of ^{238}U atoms per gram of solid and the decay constant, respectively. The activity of ^{234}Th in solution is a production–decay equation (combining Eqns. 4 and 5) of the form:

$$A_{234_{Th}} = \frac{1}{4} LSN_{238}\;\rho\lambda_{238} \times \left(1 - e^{-\lambda_{234_{Th}} t}\right) / \lambda_{234_{Th}} \tag{16}$$

All of the terms on the right side of the equation are known or can be measured independently, however, in natural systems the grain surface area (S) and its influence in directing α-recoil to the fluid phase is arguably the most important variable. For example, Kigoshi (1971) assumed spherical grain geometry for their 1–10 μm diameter zircon sand and then fit the measured ^{234}Th activities to calculate a characteristic recoil distance of 55 nm. Once L is known from similar experiments or determined by other methods, the probability of an α-particle (f_α) being ejected from a mineral grain assuming a spherical geometry can be approximated:

$$f_\alpha = \frac{3}{4}\left(\frac{L}{r} - \frac{L^3}{12r^3}\right) \tag{17}$$

Subsequent papers have explored the evolution of the solid phase and the effects of non-ideal grain geometry on the production of daughter products to the fluid phase (Kigoshi 1971; Fleischer and Raabe 1978; Fleischer 1980; 1988; Maher et al. 2004; DePaolo et al. 2006, 2012; Lee et al. 2010; Handley et al. 2013). A general conclusion from these studies, particularly those of Lee et al. (2010) and Handley et al. (2013), is that the chemical treatment of sediments and the model of grain surface structure need to be carefully considered and normalized across multiple laboratories in order for results to be broadly useful. Similar observations are noted, with important caveats for the differing chemical behavior, in the elements Th, Ra and Rn (Torgersen 1980; Semkow 1990; Sun and Semkow 1998; Porcelli and Swarzenski 2003). For example Ra is strongly adsorbed to mineral surfaces at low ionic strength but soluble at high ionic strength, thus the solution chemistry is critical for interpreting Ra activities (Moore 1976).

The general equations describing the evolution of uranium series isotopic ratios in pore fluids and minerals are presented by Ku et al. 1992; Porcelli et al. 1997; Henderson et al. 2001; Tricca et al. 2001; Porcelli and Swarzenski 2003; Maher et al. 2004. The evolution of pore fluid composition is related to primary mineral dissolution, secondary mineral precipitation reactions, α-recoil and preferential leaching of daughter isotopes to the pore fluid, sorption–desorption reactions and diffusion–advection of fluid in and out of a pore. Alpha-recoil loss, preferential leaching near the mineral surface, and solid-state diffusion, will all affect the solid composition with respect to time. However, these processes operate at different timescales, allowing mineral grains to evolve distinct ^{234}U/$^{238}U_{AR}$ domains. There is considerable discussion in the uranium series literature about the relative roles of preferential leaching and direct α-recoil leading to daughter isotope accumulation in the pore fluid (Rosholt et al. 1963; Vigier et al. 2005; DePaolo et al. 2006; Dosseto et al. 2006). Preferential leaching may occur due to mineral lattice damage associated with ^{234}Th recoil (Rosholt et al. 1963) or due to preferential oxidation of the ^{234}U in damaged mineral lattice by aqueous fluids (Kolodny and Kaplan 1970). Regil et al. (1989), Roessler (1983, 1989) and Adloff and Roessler (1991) present detailed models of ^{234}U oxidation due to α-recoil.

It is difficult to ascertain the exact mechanism that transfers ^{234}U preferentially from the solid phase to the pore fluid, but this process has important implications for the interpretation of uranium series isotopes in mineral–fluid systems. DePaolo et al. (2006) suggest that based on fine-grained alluvial sediments, the leaching depth into grains is not appreciably greater than the recoil distance. For the purposes of this discussion we proceed under the assumption that direct α-recoil is the primary mechanism of ^{234}U transfer, but acknowledge this may be unwarranted, particularly in coarser-grained or uranium rich minerals.

The mass conservation equations presented below are applied to the ^{234}U and ^{238}U isotopes and illustrated schematically for distinct pore fluid, solid surface, and solid interior compositions in Figure 3. This formulation can be applied to other intermediate daughter products with additional consideration for differing chemical behavior (e.g., strong sorption/secondary mineral partitioning of thorium and radium under certain conditions). At the scale of a single pore surrounded by mineral grain surfaces, the $^{234}U/^{238}U_{AR}$ of the fluid will evolve based on the dissolution–precipitation reactions and α-recoil ejection to the fluid.

The $^{234}U/^{238}U_{AR}$ evolution of mineral grains with time is:

$$^{234}\mathrm{U} / {}^{238}\mathrm{U}_{\mathrm{AR}} = \left(1 - f_{\alpha}\right) + \left[A_0 - \left(1 - f_a\right)\right] e^{-\lambda t} \tag{18}$$

It is apparent from Equation (18) that probability of α-particle ejection (f_α) and time are the critical variables that affect the activity ratio of the solid grains (DePaolo et al. 2006). Estimating f_α requires knowledge of the mineral volume surface area and recoil distance. DePaolo et al. (2006, 2012) calculated f_α as a function of grain diameter and shape (surface area), demonstrating, for example, that mineral grains of 10-μm diameter could have greater than a factor of 10 variability in f_α (Fig. 4).

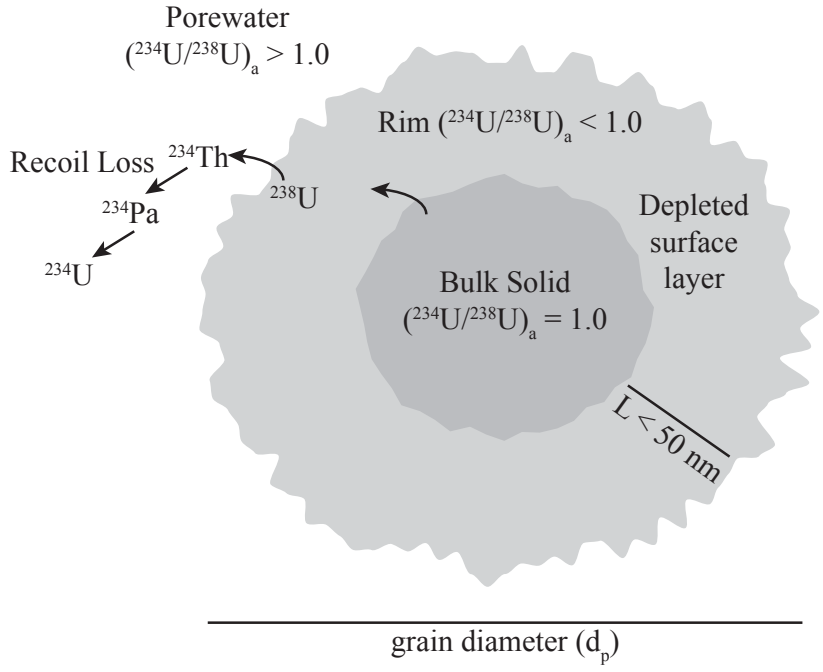

Figure 3. Mineral grains in contact with pore fluids lose ^{234}U by alpha recoil, preferential leaching along recoil tracks, dissolution-precipitation and diffusion. The recoil distance of Th (L) defines the depleted surface area depth. Adapted from Maher et al. (2006a).

A subsequent study by Bourdon et al. 2009 suggests employing a combined BET sorption surface area measurements and a fractal dimension model to overcome the uncertainty of mineral surface areas in natural sediments.

$$f_\alpha = \frac{1}{4}\left[\frac{2^{D-1}}{4-D}\left(\frac{a}{L}\right)^{D-2}\right] L \times S_{\mathrm{BET}} \times \rho \tag{19}$$

where S_{BET} is the measured surface area, a is the molecule diameter for the adsorbate and D is the fractal dimension of the grain surface, which is measured independently. Non-ideal (spherical) surface area is particularly important at the pore scale, where roughness (Lee et al. 2010) can increase the surface area of a mineral grain by a factor of 17. The sorption data of Bourdon et al. (2009) have been successfully applied to studies of soils (Oster et al. 2012) and to date ice using trapped fine-grained sediments (Aciego et al. 2011).

The evolution of $^{234}U/^{238}U_{AR}$ of pore fluids is described by Equation (20):

$$R_{\mathrm{f}}\frac{\partial A_{\mathrm{f}}}{\partial t} = R_{\mathrm{d}} M_{\mathrm{s}} \frac{C_{\mathrm{s}}}{C_{\mathrm{f}}}\left(A_{\mathrm{s}} - A_{\mathrm{f}}\right) + \left(\lambda_{238} - \lambda_{234}\right) R_{\mathrm{f}} A_{\mathrm{f}} + \lambda_{234}\left(R_{\mathrm{f}} + f_\alpha M_{\mathrm{s}} \frac{C_{\mathrm{s}}}{C_{\mathrm{f}}}\right) \tag{20}$$

where C is the concentration and A is the $^{234}U/^{238}U_{AR}$ of the solid (s) and fluid (f), R_{d} is the rate of dissolution in inverse time, R_{f} is the retardation factor accounting for sorbed uranium and M_s is the solid/fluid volume ratio (Tricca et al. 2001; Maher et al. 2004).

The conservation equation can be rearranged to yield the following approximation for the pore fluid at steady state ($A_{\mathrm{f(ss)}}$):

$$A_{\mathrm{f}(ss)} = \frac{R_{\mathrm{d}} A_{\mathrm{s}} + \lambda^{234} f_\alpha}{R_{\mathrm{d}}} \tag{21}$$

This relationship can then be manipulated to use the activity ratios to calculate the solid dissolution rate:

$$R_{\mathrm{d}} = \frac{f_\alpha \lambda^{234}}{A_{\mathrm{f(ss)}} - A_{\mathrm{s}}} \tag{22}$$

Maher et al. (2004) used this relationship to calculate the dissolution rates of deep-sea sediments over timescales longer than those accessible by laboratory experiments.

The models described above are a small sample of the work on uranium series isotopes in hydrogeologic systems. At the pore scale additional complexities may be considered, particularly when the steady-state assumption is not valid. For example, rapid changes in the dissolution rate could dissolve the ^{234}U depleted layer of mineral grains, lowering the $^{234}U/^{238}U_{AR}$ in the pore fluid. Additionally, where mineral grains are in direct contact with one another the ejected daughter isotope may be implanted into an adjacent mineral grain and not accumulated in the pore fluid. The net effect of significant implantation would be to underestimate the sediment dissolution rate (Eqn. 22) or the age of fine-grained sediments (DePaolo et al. 2006). In general the aforementioned studies demonstrate that uranium series disequilibria is largely controlled by the surface structure of individual grains that affect the isotopic composition of fluids considered at the continuum scale. Uncertainty in the relative contributions of α-recoil and preferential leaching to isotopic fractionation in the uranium series and precise measurements of mineral surface area and recoil tracks currently limit the fidelity of existing models. Future directions in this area may include incorporating daughter isotopes with different recoil distances such as ^{230}Th and ^{226}Ra to better constrain the f_α

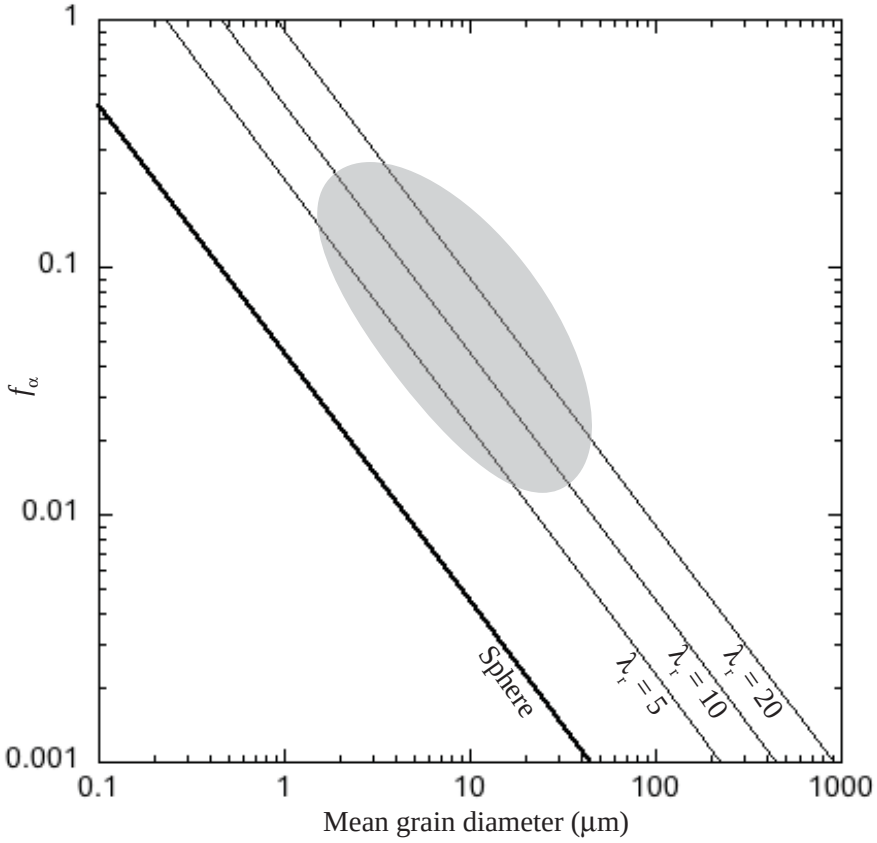

Figure 4. Estimates of f_α as a function of grain size modified from DePaolo et al. (2006), Maher et al. (2006a) and DePaolo et al. (2012). Values of λ_r represent a roughness factor accounting for deviations in grain shape and surface area from an ideal sphere. Grey shaded zone indicates the region of measured values from the King's River Fan (Lee et al. 2010), dust from ice cores (Aciego et al. 2011), marine sea core sediment (DePaolo et al. 2006) and sediment from Hanford, WA (Maher et al. 2006a).

parameter and more sophisticated imaging techniques to quantify mineral surface structure. Additionally, precise measurements of the α-recoil distance (L) and the relationship between surface area and f_α will be necessary to improve the application of pore scale $^{234}U/^{238}U_{AR}$ to diverse problems such as sediment dating, mineral dissolution rates and vadose zone transport.

Diffusive fractionation

The change in concentration (C) of a solute due to a net divergence of the flux (J) in an arbitrary volume

$$\frac{dC}{dt} = -\nabla \cdot J \tag{23}$$

is often approximated with the linear transport theory that relates the diffusive flux to the gradient in chemical potential or concentration, i.e., Fick's first law:

$$J = -D\nabla C \tag{24}$$

Here the transport coefficient D is the molecular diffusivity of the solute and has units of length squared per time.

Under ideal conditions, kinetic theory provides an expression for the diffusion coefficient of molecules in a gas

$$D = l\left(\mathrm{R}T/m\right)^{1/2} \tag{25}$$

as the product of the mean free path (l) between collisions, and the square root of the product of the gas constant (R) and temperature (T) divided by the mass (m) of the molecule or atom. This relationship suggests that the mass of the particle influences the transport coefficient and by extension the flux to the reactive surface. Therefore the lighter the particle the larger the diffusion coefficient, which leads to the expectation that if two particles differ in their masses (m_1 and m_2), then for the same conditions the difference in their diffusion coefficients would be

$$D_2/D_1 = \left(m_1/m_2\right)^{1/2} \tag{26}$$

However, this relationship is specific to an ideal gas, and in liquids the factors that contribute to the value of an individual species diffusion coefficient become much more complex (Moller et al. 2005; Yamaguchi et al. 2005). For instance, in electrolyte solutions, the influence of electrochemical forces on the interaction of diffusing species cannot be neglected, and thus requires accounting for cross-diagonal terms representing the influence of one species' or isotopic activity gradient or electrochemical potential gradient on another. This effect may be quantified in the absence of charged surfaces by including treatment of electrochemical migration using the Nernst–Plank equation (Steefel and Maher 2009; Steefel et al. 2015; Rasouli et al. 2015), while treatment of surface charge requires further inclusion of a complete electrical double layer model (Tournassat and Steefel 2015, this volume).

In the context of stable isotope fractionation in aqueous solutions, this complexity has only recently been considered. Richter et al. (2006) conducted a series of experiments to determine the fractionation of isotopes associated with diffusion in comparison with previously estimated values. Their experimental design allowed a small volume of aqueous solution containing a dissolved salt (V_1) to be suspended inside of a much larger volume of dilute fluid (V_2). The length and aperture of the tube connecting the two reservoirs was selected such that the solution inside of V_1 would remain well mixed over the timescale necessary for dissolved solutes to diffuse into V_2. Richter et al. (2006) considered departure from Equation. (26) by recasting the power as a parameter (β), which they then fit to their experimental data.

$$D_2/D_1 = \left(m_1/m_2\right)^{\beta} \tag{27}$$

The results of their study determined β values less than 0.5, but greater than 0.0, thus providing evidence that kinetic fractionation due to diffusion could contribute to observed variations in stable isotope ratios in aqueous solutions. However, their method required the implicit assumption that an inverse power law (Eqn. 27) is an accurate description of the dependence of a diffusion coefficient on the mass of the solute. Bourg and Sposito (2007) sought to directly test this assumption by utilizing molecular dynamics (MD) simulations. The use of a numerical method allowed them to obtain the diffusion coefficient for more than two isotopes of the same species, and thus test the generality of the β values reported by Richter et al. (2006). Their results showed good agreement with the Richter et al. (2006) values, demonstrating that the value of β for a given mass pair in aqueous solutions is typically less the value of 0.5 predicted

by kinetic theory for an ideal gas (Eqn. 26). Following on the agreement of these results, Bourg et al. (2010) extended both the experimental and numerical results to include additional ions. The results of these studies are summarized in Table 1.

Table 1. Experimentally and numerically determined values of β for solutes at 348 K. Summarized from Richter et al. (2006); Bourg and Sposito (2007); Bourg et al. (2010).

Solute	Measured	Measured β	MD modeled β
Li^+	$D_{^7Li} / D_{^6Li} = 0.99772$	0.0148 ± 0.0017[a]	0.0171 ± 0.0159[b]
Na^+	$D_{^{24}Na} / D_{^{22}Na} = 0.99800$	0.023 ± 0.023[c]	0.029 ± 0.022[d]
K^+	$D_{^{41}K} / D_{^{39}K} = 0.99790$[e]	0.042 ± 0.002[d]	0.042 ± 0.017[d]
Cs^+			0.003 ± 0.018[d]
Cl^-	$D_{^{37}Cl} / D_{^{35}Cl} = 0.99857$[a]	0.0258 ± 0.0144[a]	0.034 ± 0.018[b]
Br^-	$D_{^{37}Cl} / D_{^{35}Cl} = 0.99857$[a]	0.0320 ± 0.0097[f]	
Mg^+	$D_{^{25}Mg} / D_{^{24}Mg} = 1.00003$[a]	0 ± 0.0015[a]	0.006 ± 0.018[b]
Ca^{2+}	$D_{^{44}Ca} / D_{^{40}Ca} = 0.99957$[e]	0.0045 ± 0.0005[d]	0.0000 ± 0.0108[d]

Notes: [a]Richter et al. (2006); [b]Bourg and Sposito (2007); [c]Calculated by Richter et al. (2006) from measurements at 298 K from Kunze and Fuoss (1962); [d]Bourg et al. (2010); [e]Calculated based on difference in masses of measured isotopes and reported β value; [f]Calculated by Bourg et al. (2010) from measurements made between 275–353 K by Eggenkamp and Coleman (2009)

Two key aspects of these observations are that the monovalent solutes show a larger contrast in the diffusivity of their isotopes than divalent solutes, and this difference does not follow a direct correlation with the ratio of the masses. Bourg et al. (2010) demonstrated that this relationship occurs as a result of (1) the size of the solute radius, and (2) the strength of attractive interactions between the solute and solvating water (effective mass of the diffusing species), both of which influence coupling of motion between the solute and solvent. Using the residence time of water (τ) in the first solvation shell of the ion obtained from the MD simulations as a proxy for this coupling, Bourg et al. (2010) showed a clear correlation between the inverse of τ and β (Fig. 5).

The aforementioned experimental observations and MD simulations indicate that pore scale gradients in both concentration and isotopic abundance between a reactive surface and the surrounding fluid (Fig. 1) are influenced by diffusion coefficients that differ as a result of the size and charge of ions and the difference in masses of their isotopes. The effects of ion size and charge are explicitly treated at the resolution of MD simulations, but must be approximated at larger scales. Therefore accurate representation of these diffusive effects on isotopic partitioning at the pore and continuum scale requires independent knowledge of the magnitude of fractionation associated with the isotopes of each ion of interest (Table 1). Furthermore, the extent to which observed differences in diffusivity relate to fractionation associated with dispersion at larger scales is unknown.

From the results of Richter et al. (2006), Bourg and Sposito (2007) and Bourg et al. (2010), the value of β relating the ratio of the masses to the ratio of the diffusion coefficients is highly variable among ions and solution compositions. In principle, the ratio of the diffusion coefficients could be directly obtained for two isotopologues, specific to a given solution

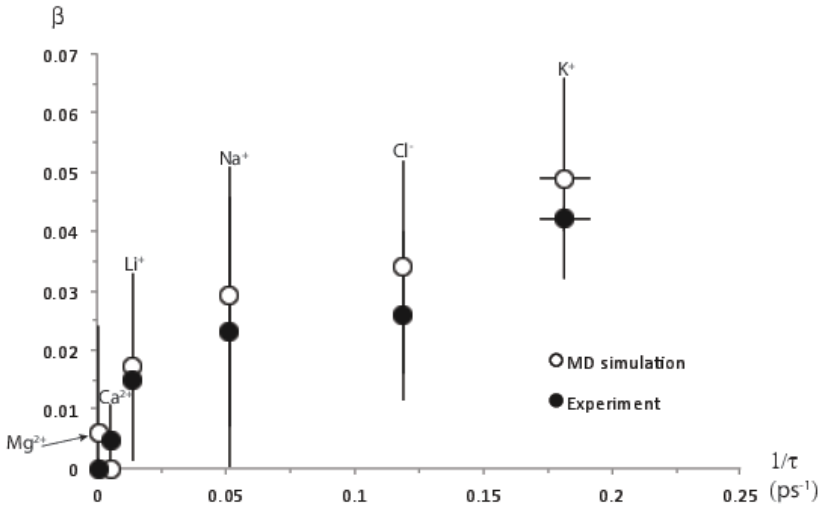

Figure 5. β values as a function of inverse residence time of water in the first solvation shell for ions where both experimental and MD simulation data are available. Figure modified from Bourg et al. (2010).

composition, through a simple diffusion experiment. For example, implementing a generic tracer in a discretized domain using the CrunchFlow (Steefel et al. 2015) reactive transport code such that at the start of the simulation an elevated concentration exists in the center of a closed system, one may obtain the spatial partitioning of the tracer as it diffuses through the system (Fig. 6A). If this total tracer is broken into two components, where one 'isotope' composes the majority of the tracer concentration and the other is a trace amount, then a slight difference in the diffusion coefficients of the two species results in a spatial profile of their ratio through time (Fig. 6B). We emphasize that this simple modeling example demonstrates a proof of concept wherein an experimental system could provide a time series of the tracer concentration (Fig. 6C) and isotope ratio (Fig. 6D) at a fixed observation point. For any system in which variation in the isotope ratios are large enough to be detected beyond measurement error, a time series dataset of this nature could be used to obtain unique values for the diffusion coefficients. If the difference in the masses of the isotopologues is known, these values could then be related to obtain direct estimates of β for a given system.

The sensitivity of isotope ratio measurements are such that diffusive fractionation may influence the interpretation of observed fractionation, but these effects have only recently begun to be considered in hydrologic studies. Analytical and numerical models have demonstrated that even in the absence of true diffusive fractionation, neglecting the effects of diffusion and dispersion leads to a lower overall estimate of reaction progress based on stable isotope ratios than when these factors are considered (Abe and Hunkeler 2006; Van Breukelen and Prommer 2008). These results have lead to a recent focus on the effects of dispersive mixing on stable isotope ratios, with particular emphasis on compound-specific stable isotope labels used to track contaminant degradation. Hydrodynamic dispersion is a fundamentally distinct process from molecular diffusion, arising from the fluctuations in velocity within and among connected pores during flow. Under certain assumptions, dispersion has been shown to display a diffusive behavior. In practice, most efforts to directly simulate fractionation due to dispersion in through-flowing systems have made use of estimated relationships between the ratio of the masses and the ratio of the dispersion coefficients. Dispersive isotope fractionation has been simulated at the continuum scale for both hydrogen and carbon isotopologues of solutes during flow through heterogeneous porous media using a variety of approximations for the difference in isotope-specific dispersivities. LaBolle et al. (2008) calculated isotope-specific

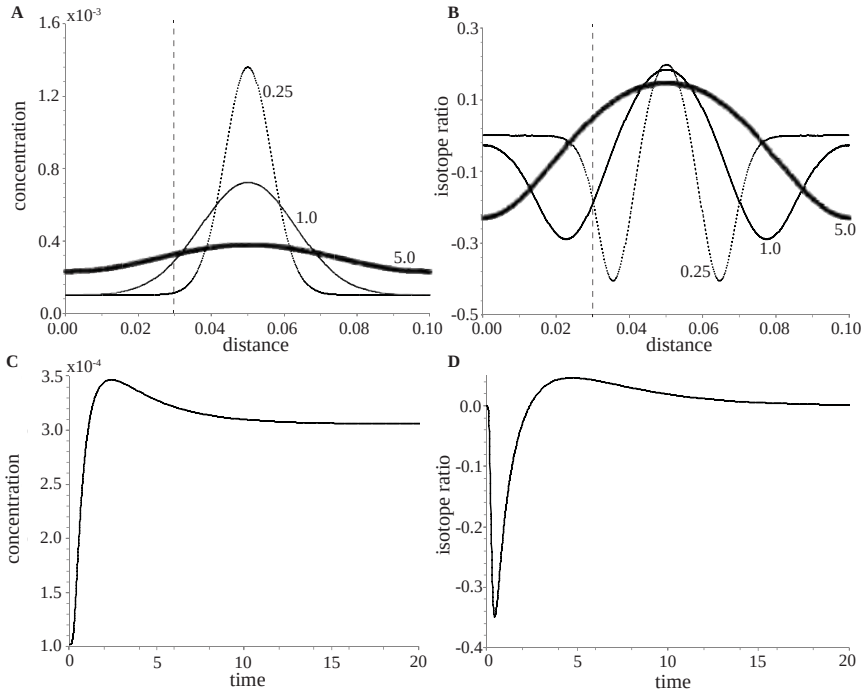

Figure 6. Numerical simulation of a tracer diffusing through time in a discretized domain demonstrating how experimental diffusion data could be used to constrain relative diffusion coefficients. The system is closed, and initially an elevated concentration exists in the center of the domain. (A) the concentration of the tracer across the domain through arbitrary time points 0.25, 1 and 5; (B) the isotope ratio relative to an arbitrary standard in delta notation (‰) for the same time points. In (A) and (B) the vertical dashed line corresponds to the location over which time series of concentration (C) and isotope ratio (D) are monitored.

values of dispersivity by substituting the reduced masses of the solutes into Equation (26). Rolle et al. (2009), Eckert et al. (2012) and Van Breukelen and Rolle (2012) used an empirical correlation from Worch (1993) close to Equation (26) but with a power of 0.53. Thus far it is not evident what, if any relationship may exist between diffusive and dispersive fractionation, or even if the power law relationship between the ratio of the masses and ratio of the diffusion coefficients validated by Bourg and Sposito (2007) holds true for the ratio of two isotopic dispersion coefficients.

Dissolution

Fractionation directly associated with the dissolution of material from the solid phase is often considered negligible over the reactive timescales represented by many natural samples. This assumption is justified in that many of the mechanisms thought to contribute to isotopic partitioning, such as transport (discussed above), and changes in solvation (Hofmann et al. 2012), are restricted within a solid phase. Furthermore, where apparent shifts in isotopic ratio are observed during net dissolution of natural samples, it is difficult to distinguish preferential mobilization of individual, isotopically distinct mineral phases from true fractionation (Ryu et al. 2011). However, a wide variety of studies now appear to demonstrate observable fractionation during dissolution, usually during the initial stages. These observations are significant in that they implicitly require that the solid become isotopically differentiated as material is removed from the reactive surface. This implies the development of a surface that is compositionally distinct from the interior of the grain, a process that is not readily compatible with bulk or volume fraction representations of solids.

The earliest observations of fractionation during dissolution involved dissimilatory reduction of ferric iron by anaerobes (Beard et al. 1999, 2003; Brantley et al. 2001, 2004), which naturally led to the issue of whether observed iron isotope partitioning was a vital effect or if it could be reproduced in abiotic systems. From this starting point, a wide range of experimental conditions, including both pure mineral phases and whole rocks, as well as a variety of stable isotope ratios, have shown evidence for partitioning of isotopes during net dissolution (Table 2). The compilation in Table 2 is limited to low temperature and ambient pressure experimental conditions in which efforts have been made to minimize fractionation of fluid phase isotopes due to additional effects, such as secondary mineral precipitation.

Despite wide variability in experimental conditions, a common observation is that during dissolution the isotopic composition of the fluid phase tends to be lighter than that of the initial solid, i.e. the light isotope tends to be preferentially dissolved. Furthermore, in studies where the isotopic value of the fluid is monitored as a function of time, the magnitude of this fractionation appears to vary. When a solid is introduced to an aqueous solution such that the system is undersaturated, the fractionation between the fluid and solid phase tends to exhibit a maximum value relatively soon after the experiment is initiated (Fig. 7). For example, the dissolution of goethite at pH 3 (Wiederhold et al. 2006) promoted by ligand complexation leads to a maximum fractionation between dissolved Fe and the bulk solid of -1.83‰, but this difference lessens as dissolution continues (Fig. 7A). A similar temporal trend is noted in iron isotopes during proton-promoted dissolution of granite (Kiczka et al. 2010)(Fig. 7b), in zinc isotopes during both proton and ligand promoted dissolution of biotite (Weiss et al. 2014) and in silicon isotopes during proton promoted dissolution of Hawaiian basalt (Ziegler et al. 2005). At higher temperatures and pressures, the same trend is noted in lithium isotopes during the dissolution of basalt (Verney-Carron et al. 2011) and in magnesium isotopes during the dissolution of basalt and forsterite (Wimpenny et al. 2010), but magnesium isotopes show the opposite behavior during magnesite dissolution (Pearce et al. 2012). A low-temperature exception to this general trend may be the fractionation of copper isotopes associated with oxidative dissolution of sulfide minerals. Mathur et al. (2005) reported Δ^{65}Cu values of +2.74‰ and +1.32‰ for the abiotic dissolution of chalcocite and chalcopyrite, respectively. They suggested this isotopic enrichment of the solute was associated with the accumulation of secondary phases, however, a subsequent study demonstrating +2.0‰ values for dissolution of whole rock containing chalcopyrite argued that secondary mineral formation was negligible (Fernandez and Borrok 2009).

The general observation of an initially negative $\Delta_{\text{fluid–bulksolid}}$ value that trends towards zero with further reaction progress is common to a variety of reactive pathways, minerals and isotope systems, and is observable even during dissolution of natural samples. For example, the biotite and chlorite enriched component of a granite sample dissolved in the presence of hydrochloric and oxalic acids demonstrated negative $\Delta_{\text{fluid–solid}}$ values that were most pronounced early in the reaction (Kiczka et al. 2010) (Fig. 7B). This study explored a range of dissolution rates by varying the potassium concentration, which served to slow down the rate of iron release in the HCl experiments, and observed a greater enrichment in the light isotopes of the fluid phase with decreasing dissolution rate. In contrast, addition of potassium to the oxalic acid experiments only made a small difference in the Fe release rates, and little difference in the $\Delta_{\text{fluid–bulksolid}}$ values were observed. Reaction of a biotite granite with the same acids yielded similar temporal trends, though the maximum $\Delta_{\text{fluid–bulksolid}}$ values showed lighter isotope composition for the fluid phase with more acidic solutions (Chapman et al. 2009). These observations suggest that the partitioning of stable isotopes may potentially be utilized as an indicator of the mechanisms of mineral weathering, leading to development of a variety of conceptual and quantitative models for fractionation during congruent dissolution.

Table 2. Compilation of measured fractionation between dissolved and initial solid phases during net dissolution at ambient temperature and pressure. Where fractionation is measured as a function of time, the maximum value is reported. Values are divided into abiotic and microbially mediated experimental conditions. Values reported in italics are considered within error of 0.0‰.

Isotope ratio	Solid phase	Reactant or bacterium	Stirred/ shaken	T (°C)	Initial pH	Max $\Delta_{fluid-solid}$ ‰	Ref.
$\delta^{7}Li$	forsterite	HCl	yes	25	2–3	*+1.6*	[1]
$\delta^{7}Li$	basalt glass	HCl	yes	25	3	*-3.3*	[1]
$\delta^{26}Mg$	forsterite	HCl	yes	25	2–3	-0.37	[1]
$\delta^{26}Mg$	basalt glass	HCl	yes	25	3	-0.21	[1]
$\delta^{30}Si$	Hawaiian basalt	HCl	no	*	3	-2.5	[2]
$\delta^{56}Fe$	granite	HCl	yes	22	4	-0.55	[3]
$\delta^{56}Fe$	granite	HCl	yes	22	2	-0.51	[3]
$\delta^{56}Fe$	granite	HCl + 0.5 mM K	yes	22	4	-1.15	[3]
$\delta^{56}Fe$	granite	HCl + 5 mM K	yes	22	4	-1.25	[3]
$\delta^{56}Fe$	granite	oxalic acid	yes	22	4.5	-0.40	[3]
$\delta^{56}Fe$	granite	oxalic + 0.5 mM K	yes	22	4.5	-0.49	[3]
$\delta^{56}Fe$	granite	oxalic + 5 mM K	yes	22	4.5	-0.37	[3]
$\delta^{56}Fe$	biotite granite	HCl	**	22	0.34	-1.85	[4]
$\delta^{56}Fe$	biotite granite	oxalic acid	**	22	2.18	-1.33	[4]
$\delta^{56}Fe$	tholeiite basalt	HCl	**	22	0.34	-1.52	[4]
$\delta^{56}Fe$	tholeiite basalt	oxalic acid	**	22	2.18	-0.82	[4]
$\delta^{57}Fe$	goethite	HCl	yes	*	0.3	-0.17	[5]
$\delta^{57}Fe$	goethite	oxalic (dark)	yes	*	3	-1.86	[5]
$\delta^{57}Fe$	goethite	oxalic (light)	yes	*	3	-2.44	[5]
$\delta^{56}Fe$	hornblende	acetic acid	yes	*	n.r.	-0.96[a]	[6]
$\delta^{56}Fe$	hornblende	citric acid	yes	*	n.r.	-1.22[a]	[6]
$\delta^{56}Fe$	goethite	siderophore	no	*	n.r.	*+0.21*[a]	[6]
$\delta^{56}Fe$	hornblende	oxalic acid	no	*	n.r.	-0.25[a]	[7]
$\delta^{56}Fe$	hornblende	siderophore	no	*	n.r.	-0.36[a]	[7]
$\delta^{66}Zn$	biotite granite	HCl	yes	*	0.34	-1.24	[8]
$\delta^{66}Zn$	biotite granite	oxalic acid	yes	*	2.18	-1.15	[8]
$\delta^{56}Fe$	hematite	*Shewanella*	n.r.	30	6.8	-2.04	[9]
$\delta^{56}Fe$	goethite	*Shewanella*	n.r.	30	6.8	-0.95	[9]
$\delta^{56}Fe$	hematite	*Geobacter*	n.r.	30	6.8	-2.09	[9]
$\delta^{56}Fe$	goethite	*Geobacter*	n.r.	30	6.8	-0.93	[9]
$\delta^{56}Fe$	hematite	*Shewanella*	no	*	n.r.	-1.3[a]	[10]
$\delta^{56}Fe$	goethite	*Bacillus*	no	*	n.r.	-1.44[a]	[6]
$\delta^{56}Fe$	hornblende	*Bacillus*	no	*	n.r.	-0.56[a]	[7]
$\delta^{56}Fe$	hornblende	*Streptomyces*	no	*	n.r.	-0.48[a]	[7]
$\delta^{56}Fe$	ferrihydrite	*Shewanella*	no	*	n.r.	-1.3[a]	[11]

Notes: *reported as ambient room temperature; **shaken once every 24 hours; [a] no time series reported

[1] Wimpenny et al. (2010) [2] Ziegler et al. (2005) [3] Kiczka et al. (2010) [4] Chapman et al. (2009) [5] Wiederhold et al. (2006) [6] Brantley et al. (2004) [7] Brantley et al. (2001) [8] Weiss et al. (2014) [9] Crosby et al. (2007) [10] Beard et al. (2003) [11] Beard et al. (1999)

The preferential removal of light isotopes during the initial stages of a dissolution reaction is commonly considered a kinetic fractionation associated with enrichment of the solid surface in the heavy isotope. Some studies have considered whether or not the initial stage in which this surface layer is established could be described as a distillation or Rayleigh process. Wiederhold et al. (2006) discussed this conceptual model in the context of iron isotopes and Weiss et al. (2014) in the context of zinc isotopes. Both studies point out that a Rayleigh model would carry the implicit assumption that the isotopes of the solid phase are well mixed, and thus homogeneously released. However, the development of either a depth into the solid that is isotopically zoned or a non-uniform distribution of reactive surface sites along a monoatomic surface layer both contradict this requirement. The consistent observation of a maximum $\Delta_{\text{fluid–bulksolid}}$ early in the reaction progress that becomes less depleted with time (Fig. 7) then requires consideration of an additional mechanism.

The development of an isotopically distinct solid surface has been modeled in terms of the propagation of a reacted surface layer into the unreacted solid. This is based on the idea of a preferentially reacted or 'leached' layer as commonly used to describe non-stoichiometric dissolution of silicates, e.g., Casey et al. (1993); Casey and Ludwig (1996); Hellmann et al. (1990); Oelkers (2001). Brantley et al. (2004) derived a model for isotopic fractionation

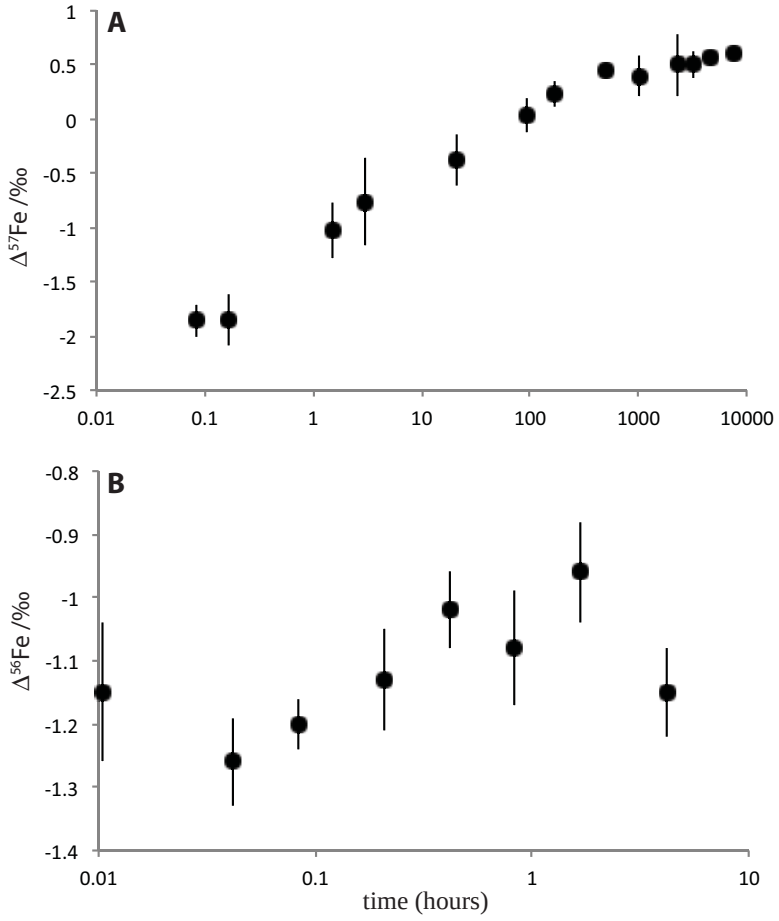

Figure 7. Fractionation between dissolved and bulk solid iron isotopes as a function of time since the start of dissolution. A Δ-value of 0.0 represents no fractionation. (A) Goethite dissolution promoted by oxalate in the absence of light, which removes the effects of oxidation, modified from Wiederhold et al. (2006). (B) Granite (biotite and chlorite enriched fraction) dissolution promoted by hydrochloric acid, modified from Kiczka et al. (2010).

during dissolution based on a transfer of material from the bulk solid through a layer altered by dissolution to the fluid. The depth of the altered surface layer (x), the flux of material from the bulk solid to this layer (F) and the rate of dissolution from the surface layer to the fluid ($R = kC(t)$) all contribute to the transient value of $\Delta_{\text{fluid–bulksolid}}$ (Fig. 8A). The model is given as a ratio of the rates of ^{54}Fe and ^{56}Fe entering the fluid phase:

$$\frac{^{54}R}{^{56}R} = \frac{\left[\left(^{54}F / x\right)\left(1-\exp\left(-^{54}kt\right)\right) + {}^{54}k\,{}^{54}C_o\exp\left(-^{54}kt\right)\right]}{\left[\left(^{56}F / x\right)\left(1-\exp\left(-^{56}kt\right)\right) + {}^{56}k\,{}^{56}C_o\exp\left(-^{56}kt\right)\right]} \tag{28}$$

where ^{54}k and ^{56}k are the rate constants for the dissolution of material from the surface layer to the fluid for ^{54}Fe and ^{56}Fe, respectively. Similarly $^{54}C_o$ and $^{56}C_o$ are the respective concentrations of the isotopes of iron in the bulk solid and t is the time since dissolution started. As discussed in Brantley et al. (2004), this equation effectively describes the period of time from the start of dissolution to the establishment of a steady state value for a given surface layer depth (x) (Fig. 8B and C). At very early time, relative rates of dissolution of the two isotopes are governed by the ratio of the rate constants, but as time progresses, the flux from the unreacted solid to the surface layer becomes more influential and eventually controls the composition of material transferred to the fluid. Conceptually, this transition occurs because at $t = 0$, the surface layer has not been formed yet and the fluid is in contact with the bulk solid, allowing for preferential release of one isotope vs. another as a function of the ratio of the rate constants. As the surface layer develops and eventually reaches steady state, the transfer of material to this layer from the underlying, unreacted solid becomes the governing rate. In the Brantley et al. (2004) model, this steady state value is achieved quickly if the thickness of the surface layer

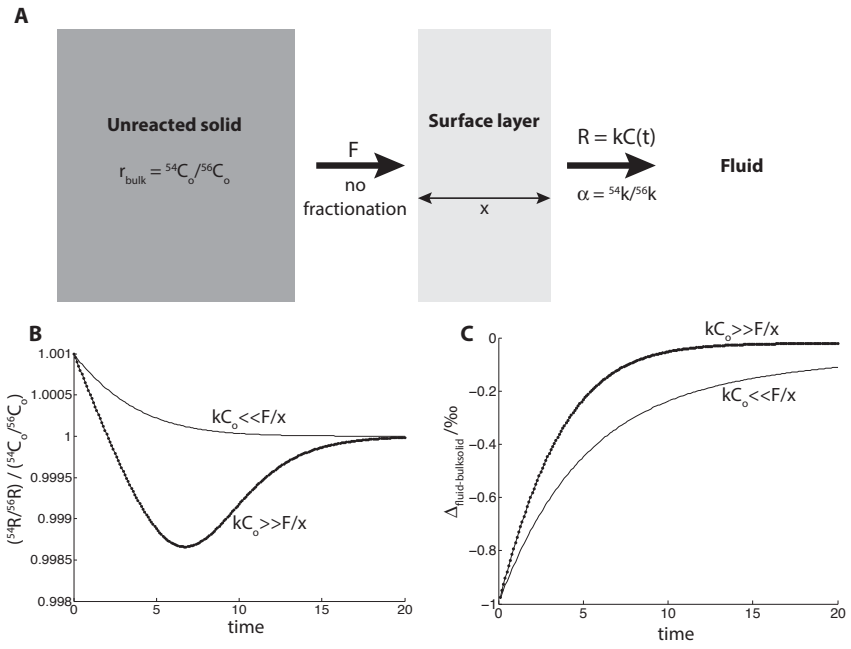

Figure 8. (A) Diagram of modeled reservoirs and material transfer describing parameters of the Brantley et al. (2004) derivation. See main text for definition of variables. (B) Ratio of release rates of iron isotopes to the fluid, relative to ratio of isotopes in bulk solid as a function of time. This value is influenced by the thickness of the leach layer, the rate of transfer of material from the bulk solid to this leach layer, and the rate of dissolution into the fluid. (C) $^{54}C(t)$ and $^{56}C(t)$ obtained by numerical integration of eq. 12 presented as $\Delta_{\text{fluid–bulksolid}}$ vs. time. Results are presented for arbitrarily chosen values $^{56}k = 0.5$, $^{54}k/^{56}k = 1.001$, ^{56}Co = 4, ^{54}Co/^{56}Co = 0.001, $F = 1$, $x = 0.01$ and 20.

is large, if the migration of this reacted surface layer into the unreacted solid is slow, or if rate of dissolution from the surface into the fluid is fast.

This model approach clearly yields a temporal trend comparable to those observed during many of the dissolution experiments discussed in the observations section (Table 2). Furthermore, it suggests that the establishment of a steady state value is independent of the fraction of solid that is mobilized, but is rather a function of the establishment of a steady state leach layer. This implies that the trend towards a $\Delta_{\text{fluid–bulksolid}}$ of approximately 0.0‰ as dissolution progresses is not the result of a depletion in the abundance of the preferentially released isotope (i.e., a mass balance restriction) but rather a shift from the influence of dissolution (into the fluid) to the influence of material transfer (into the leach layer). There are some aspects of the assumptions built into this model that may be further developed. For example, the thickness of the leach layer is fixed and allowed to propagate inward throughout the simulation, but one may conceptualize a period at the very beginning of the model in which the distinct surface layer has yet to establish and thus $x = 0$. This would then require consideration of a period over which the surface layer grows into the solid and establishes a fixed depth. Furthermore, in Equation (28) an eventual $\Delta_{\text{fluid–bulksolid}}$ value of 0.0‰ results from a flux of Fe from the bulk solid to the surface layer (F) that is non-fractionating. This distinction between the mechanism through which iron is supplied to the leach layer and the mechanism by which it is dissolved into solution are potentially difficult to reconcile, and may benefit from consideration of solid state diffusion through the reacted zone (Verney-Carron et al. 2011).

Recent analytical developments have supported increasingly high-resolution observations of the structure and chemical composition of solid surfaces and a corresponding refinement in the conceptual model of reacted zones. Nano-scale resolution of reactive fronts are becoming more commonly described as a dissolution–reprecipitation process (Hellmann et al. 2012, 2015) leading to formation of a distinct, often amorphous phase at the solid surface. The extent to which the Brantley et al. (2004) model might be reworked to consider fractionating dissolution in systems where a reacted surface layer does not form has only recently begun to be addressed. Wiederhold et al. (2006) quantified stable isotope partitioning during dissolution of a solid phase that does not form an observable reacted surface layer using a model they describe as conceptually similar to the Brantley et al. (2004) approach. In their derivation for iron isotope partitioning during goethite dissolution, the reacted surface depth was replaced by a percentage of the total iron contained in the solid phase that was considered to exist within a reactive, monoatomic surface layer. The isotopes of iron could be preferentially removed from the reactive surface sites at the step-edge of this receding monoatomic layer, but are replenished by the isotopic composition of the bulk solid. Their derivation results in two free parameters, the fractionation associated with dissolution of Fe from the reactive surface layer and the percentage of the total solid phase Fe composing the reactive surface site pool. Importantly, they fit these two parameters and obtained a best estimate for the reactive surface site pool (2.4%) that matched quite closely with the value they independently quantified based on the surface site density, the measured surface area, and the molar mass of goethite (2.7%). This model was successfully extended by Kiczka et al. (2010) to consider the contribution of two independent types of reactive surface site in a more complex granite consisting of enriched biotite and chlorite fractions.

Macroscopic or Darcy-scale reactive transport models are now becoming a common means of quantifying stable isotope partitioning by separating the isotopes of interest into individual ‘species’ that follow parallel reaction networks. The fractionating reaction in these simulations is commonly a homogeneous aqueous process (Dale et al. 2009; Gibson et al. 2011; Druhan et al. 2012, 2014; Jamieson-Hanes et al. 2012; Wanner and Sonnenthal 2013). To date, models designed to simulate the influence of dissolution on the isotope ratio of fluids

rely on the assumption that the solid-phase isotopic composition remains fixed over time. In doing so, dissolution of the solid acts as a source to the fluid phase that is isotopically invariant with time (Steefel et al. 2014a; Wanner et al. 2014). This approach is necessary given that at the continuum scale mineralogy is described as a volume fraction of the total solid in each grid cell, and thus does not readily support the development of an isotopically zoned mineral surface. Some approximation to this zoning might be achievable through the use of a nested-grid or multiple interacting continua approach (e.g., Xu and Pruess 2001), but this would severely restrict the size of the spatial domain and would require independent, *a-priori* knowledge of the length scales of zoning. Specifying a fixed isotopic composition of a solid phase also restricts the range of saturation states that can be accurately simulated. If a system were to become supersaturated with respect to a solid phase where the isotopic composition of that solid was pre-specified, accumulation of new precipitate would induce fractionation of the surrounding fluid. Stated differently, specifying a fixed solid phase isotopic composition effectively means that the rate law describing the dissolution of that solid is no longer inherently reversible.

The observed temporal trend in fractionation associated with dissolution indicates that these effects are likely negligible to long term processes, but potentially influential over shorter time periods. This implies that models for isotope fractionation applied to contaminant remobilization, microbially catalyzed oxidative dissolution and system response to short term environmental perturbations may benefit from an improved capability to simulate the isotopic partitioning characteristic of the initial stages of dissolution. Based on current modeling approaches, it appears that accounting for fractionation due to dissolution of a solid within a reactive transport framework requires a means of describing the development of a distinct solid surface that influences isotopic partitioning. This implies the need to resolve the geometry and surface of individual grains, i.e., a pore-scale model. Precipitation is less problematic, and has been more extensively described by Darcy-scale simulations, but as will be discussed in the next section this process is also influenced by the unique composition of the reactive interface.

Precipitation

In the previous section concerning studies of net dissolution, experimental conditions largely prohibited the accumulation of secondary minerals. Where secondary solids composed of the fractionating element were able to form, precipitation likely influenced the observed stable isotope ratio. For example Mathur et al. (2005) observed partitioning of copper stable isotopes during abiotic oxidative dissolution of chalcocite and chalcopyrite where the $\Delta^{56}Cu_{fluid-bulksolid}$ was positive, in conjunction with mass balance calculations that suggested removal of copper from solution. Similarly, Wimpenny et al. (2010) report positive $\Delta_{fluid-bulksolid}$ values for lithium when the pH range allowed for concurrent secondary mineral precipitation.

The formation of a precipitate from solution is broadly recognized as a fractionating mechanism in a variety of stable isotope systems. For example, partitioning of the lighter ^{6}Li isotope into the solid phase was predicted by *ab initio* calculations (Yamaji et al. 2001) and observed during carbonate precipitation (Marriott et al. 2004), clay formation (Williams and Hervig 2005; Vigier et al. 2008) and accumulation of secondary silicates (Wimpenny et al. 2010). These observations suggest that precipitation of secondary minerals contributes to enrichment in heavy lithium isotope in rivers relative to primary mineralogy in a wide variety of weathering environments (Vigier et al. 2009; Lemarchand et al. 2010; Millot et al. 2010; Dellinger et al. 2014). Similar partitioning of silicon isotopes associated with precipitation was predicted (Meheut et al. 2007, 2009) and inferred from observations of progressive basalt weathering (Ziegler et al. 2005; Georg et al. 2007) and riverine composition (Georg et al. 2006; Opfergelt et al. 2013). Recently, Geilert et al. (2014) demonstrated a temperature dependent preferential incorporation of the lighter isotope of silicon into amorphous silica, while Oelze et al. (2015) demonstrated a rate dependence of silicon fractionation during sequential

precipitation of amorphous silica in the presence of dissolved aluminum. Johnson (2011) noted that in general the isotopic partitioning of redox sensitive elements are governed by pathways that alter the redox state of reacting species, and thus precipitation in the absence of electron transfer tends to impart comparatively minor fractionation in these systems. However, Skulan et al. (2002) demonstrated that under extremely rapid precipitation rates kinetic effects were observable in iron isotopes.

The Skulan et al. (2002) study offers a closed-system kinetic end-member example of the isotopic partitioning associated with precipitation. They utilized experimental conditions in which dissolved ferric iron was rapidly precipitated from solution to form hematite, resulting in approximately 80% removal of $Fe(III)_{aq}$ in one hour. These conditions lead to a large kinetic fractionation (Fig. 9A), which was observable in both the residual aqueous phase and the bulk hematite stable isotope ratios of iron. This observation was considered a kinetic effect due to the rapid rate of accumulation prohibiting isotopic equilibration between phases and because long-term exposure of hematite to solution resulted in small $\Delta^{56}Fe$ values. Furthermore, enrichment in the heavy isotope composition of the fluid as the reaction progressed followed a Rayleigh model (Eqn. 14), adhering to an apparently constant fractionation factor of $\alpha = 0.99868 \pm 12$ and suggesting the influence of a single fractionating process. This distillation effect was pronounced enough that the shift in isotopic ratio as a function of reaction progress was also observable in the $\Delta^{56}Fe$ of the bulk hematite. Although this cumulative value only increased by approximately 0.8 ‰ compared with a fluid enrichment of roughly 4.4 ‰, mass balance dictates that the isotope ratio of the hematite surface forming from the surrounding fluid varied as much as the fluid phase, leading to formation of a solid that was isotopically heterogeneous, or zoned. This zoning was evident when hematite crystals synthesized by this rapid process were subsequently dissolved in HCl (Fig. 9B). Despite a bulk hematite $\delta^{56}Fe$ composition of -0.29 ±0.05 ‰, dissolution of the first 6.8 % of the solid yielded a fluid value of +1.16 ± 0.11 ‰, which subsequently decreased with continued dissolution to reach the value of the bulk solid.

Two aspects of the Skulan et al. (2002) results are relevant to the current discussion. First, a solid phase can preserve an isotopic signature associated with the kinetic effects of formation, and second in a closed system the kinetic signal imparted during formation of the solid phase varies as a function of the progress of the reaction, which in turn produces an isotopically heterogeneous or zoned precipitate. Dissolution of such a solid could then lead to the appearance of fractionation as an artifact of zoning. This concern was noted in several

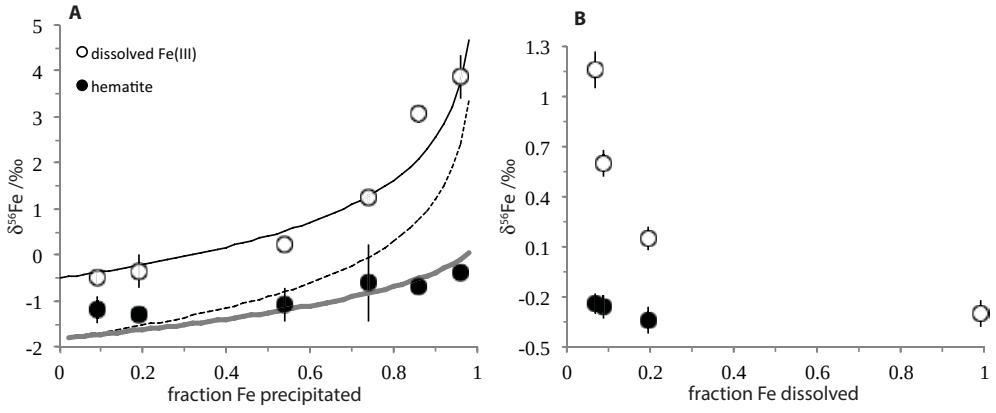

Figure 9. (A) measured values of fluid-phase $\delta^{56}Fe$ (open circles) and cumulative solid-phase $\delta^{56}Fe$ of hematite (filled circles) during rapid precipitation. Modeled fluid-phase isotope fractionation (black line, Eqn. 14) and cumulative solid-phase fractionation (grey line) agree with measured values. Modeled solid surface isotopic composition (dashed line) is inferred by mass balance. (B) corresponding values during subsequent dissolution. Data from Skulan et al. (2002).

of the dissolution studies discussed in the previous section, for example Crosby et al. (2007) conducted separate partial dissolution measurements to ensure the homogeneity of their hematite and goethite samples. Based on the Skulan et al. (2002) results, if the light isotope is preferentially incorporated into the solid during precipitation, and this solid is subsequently dissolved, zoning would seem to counteract the general trend of light isotopes preferentially mobilizing in the fluid phase during dissolution (Table 2). The extent to which preferential mobilization of the light isotope influenced the values shown in Fig. 9B cannot be disentangled from the effect of the zoned hematite composition.

If the Skulan et al. (2002) results represent one extreme, in which the isotopic composition of a precipitate is entirely governed by unidirectional, kinetic fractionation, then the other end member is the formation of a solid at slow enough rates that isotopic equilibrium is maintained between phases. Many natural systems exist in a range of saturations close to chemical equilibrium (Helgeson et al. 1984) and solids are thus often anticipated to form over timescales sufficient to reflect isotopic equilibrium. For example, the use of stable isotope ratios as paleoproxies commonly requires that the timescales associated with formation of solids are sufficient to maintain isotopic equilibrium. This has been a particular issue in the interpretation of carbon and oxygen isotope compositions in carbonates, where multiple studies have demonstrated a combination of equilibrium and kinetic effects (Romanek et al. 1992; Kim and Oneil 1997; Chacko et al. 2001; Mickler et al. 2006; Dietzel et al. 2009; Gabitov et al. 2012; Gabitov 2013; Watkins et al. 2013). More recently, the same issues have been considered in the mid-mass stable isotope ratios of cations in carbonates (Fantle and Tipper 2014). For example both magnesium and calcium isotopes have been shown to partition during carbonate mineral formation, typically such that the fluid is isotopically heavy relative to the solid (Galy et al. 2002; Lemarchand et al. 2004; Gussone et al. 2005; Tang et al. 2008; Kisakuerek et al. 2009; Immenhauser et al. 2010; Rustad et al. 2010; Reynard et al. 2011; Wombacher et al. 2011; Mavromatis et al. 2013).

Observations of both light- and mid-mass stable isotope partitioning during carbonate precipitation seem to indicate a combination of kinetic and equilibrium effects. These observations imply that the mechanisms of fractionation should not be viewed as a binary system, but rather as a continuum between the two processes. As a result, a range of reaction rates should exist near equilibrium where the apparent or observed fractionation factor associated with formation of a solid phase is rate dependent (Fig. 10). Within a closed system, this effect leads to the accumulation of an isotopically heterogeneous solid as a function of both changes in reaction rate and distillation of the reactant reservoir. Within open systems, in the absence of any supply or transport limitations, the isotopic composition of the solid surface may still vary as a result of changes in the saturation state of the system. Thus experiments designed to quantify the magnitude of isotopic partitioning between a fluid and precipitating solid often utilize open systems in which the chemical composition of the fluid is continually titrated to maintain a fixed saturation state (Tang et al. 2008; Watkins et al. 2013), thereby ensuring that the accumulated solid phase is isotopically homogeneous. In natural systems, lack of such controls on saturation state or reaction rate lead to the formation of solids such that the observed fractionation factor appears to vary both spatially (e.g., Tipper et al. 2012) and temporally (e.g., Druhan et al. 2013). Therefore models that describe the exchange of material between a coevolving fluid and solid surface should be capable of describing this variability.

Several models have been proposed for the partitioning of stable isotopes during net precipitation under controlled experimental conditions. Tang et al. (2008) utilized the surface entrapment model (SEMO) developed by Watson and Liang (1995) and Watson (2004) to describe their variable fractionation factor as a function of precipitation rate (Fig. 10). The SEMO model was developed to describe zoning of trace elements and isotopes in solids that

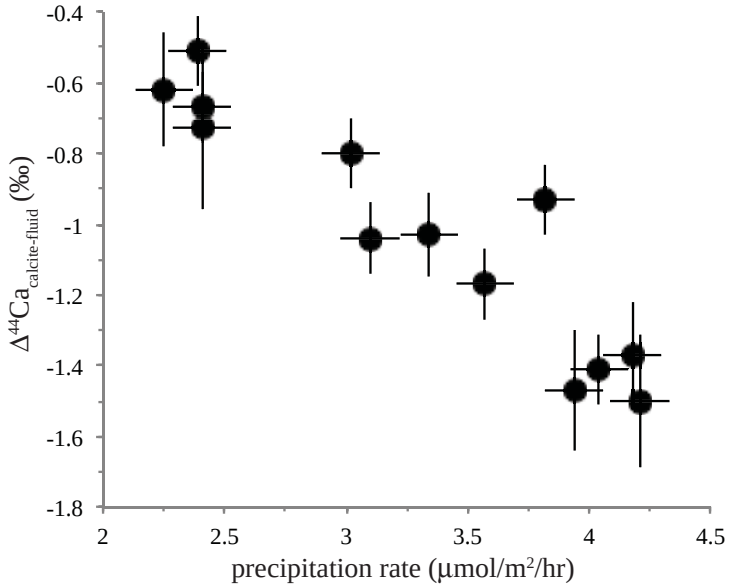

Figure 10. Calcium isotope fractionation between bulk fluid and calcite precipitated at steady state for a range of net precipitation rates (Tang et al. 2008). Each of these values are generated by precipitating calcite at a fixed oversaturation for a period of time sufficient to accumulate enough isotopically homogeneous solid for measurement.

were thought to form under such slow growth rates that the fluid and solid surface must reflect equilibrium partitioning and an absence of aqueous transport limitations. In order to explain such observations, the SEMO model assumes that although the isotope ratios of the interior of the solid and the bulk fluid reflect the equilibrium fractionation factor, there exists a surface layer of the solid in which the rare isotope is depleted, with a maximum partitioning defined by a surface entrapment factor (F). Under growth conditions, this depleted surface layer may become 'entrapped' in the crystal beneath newly formed solid, leading to a disequilibrium fractionation. This effect is offset by re-equilibration due to diffusion within the crystal lattice. A key aspect of the model is the requirement that ion mobility, in this case cast as the solid-state diffusion coefficient governing re-equilibration (Watson 2004), increases from the crystal interior to a higher value at the solid surface. In application this approach was able to accurately reproduce the trend in fractionation as a function of precipitation rate for the Tang et al. (2008) dataset. However, the diffusion coefficient at the solid surface required to achieve this result was roughly 16 orders of magnitude higher than that estimated for trace element diffusion in calcite.

An alternate approach to the SEMO model was proposed by DePaolo (2011), which considers a kinetic effect in the fluid boundary layer surrounding the precipitating solid (Fantle and DePaolo 2007). This model represents a fundamental shift from both the SEMO approach and the models used to describe dissolution discussed in the previous section, in that there is no description of a depth or volume percentage considered to represent a reactive surface. Instead, the only aspect of the solid considered is the surface in contact with the surrounding fluid (Fig. 11A), which dictates the isotopic composition of the backward reaction. As discussed in the introduction it is the cumulative effect of an irreversible forward addition of material to the mineral surface and an irreversible backward removal of material from the mineral surface that influences the observable fractionation factor, despite the fact that the overall system is supersaturated and thus precipitate is accumulating. In principle, this creates a coupled parameter set, in that the isotope ratio of the fluid and the solid surface are both evolving

and dependent on one another. DePaolo (2011) simplifies this relationship by assuming that the isotopic composition of the solid surface is at steady state, as in the case of the buffered titration experiments in which a fixed supersaturation is maintained (Tang et al. 2008; Watkins et al. 2013). In doing so, the formulation leads to a closed form solution for the observed fractionation factor (α_{obs}) at steady state

$$\alpha_{obs} = \frac{\alpha_f}{1 + \frac{R_b}{R_f}\left(\frac{\alpha_f}{\alpha_{eq}} - 1\right)} \tag{29}$$

where R_f and R_b are the forward and backward reaction rates (note R_f may be recast as $R_{net} + R_b$ to utilize the net observed reaction rate), α_f is the fractionation factor associated with the forward addition of material to the precipitating mineral and α_{eq} is the fractionation factor associated with dynamic equilibrium between the solid surface and surrounding fluid. In order to apply this model, the value of the backward rate of material removed from the solid surface, as well as the two fractionation factors α_f and α_{eq} must be supplied. DePaolo (2011) demonstrated that for an R_b of 2.16×10^3 μmol/m^2/hr roughly corresponding to the values reported by Chou et al. (1989) and fractionation factors $\alpha_f = 0.9984$ and $\alpha_{eq} = 0.9995$ the model captures the trend observed by the Tang et al. (2008) study (Fig. 11B).

This model is based on the same concept of a dynamic system discussed in the introduction section. An implicit assumption of this affinity-based approach is that reactivity and fractionation are describable based on the composition of the fluid phase relative to equilibrium with the solid. In practice, the parameters required to apply this type of model often vary between systems, for example requiring a higher order dependence on the departure from equilibrium, or a distinct kinetic rate constant (Stack 2014). DePaolo (2011) points out that the value of α_{eq} used to reproduce the Tang et al. (2008) dataset (0.9995) is inconsistent with independent estimates (Fantle and DePaolo 2007; Jacobson and Holmden 2008). An alternate parameter set is also able to fit the Tang et al. (2008) data using an α_{eq} of 1.000 and a variable backward reaction rate (R_b), which DePaolo (2011) calculates as a function of the fluid saturation state.

Recent efforts have focused on replacement of the TST derivation with crystal growth models that include a description of the type and prevalence of reactive sites at the mineral surface in an effort to provide a more mechanistic and predictive capability (Wolthers et al. 2012; Bracco et al. 2013). This type of crystal growth model has been applied in combination with the model of DePaolo (2011) to derive solutions for calcium isotope partitioning during calcite precipitation as a function of solution stoichiometry (Nielsen et al. 2012) and for oxygen isotope partitioning during calcite precipitation as a function of pH (Watkins et al. 2013). The key development of the recent modeling approaches is to allow the influence of factors in addition to reaction affinity to influence the reaction rate and thus the isotopic compositions of the fluid and solid. However, these derivations still largely incorporate a steady state solution as demonstrated in Figure 11. Recently, Steefel et al. (2014a) discuss the need to explicitly describe the time-variant evolution of both the fluid and solid surface in order to model isotopic re-equilibration of a kinetically fractionated system. In the following section, we describe current modeling approaches to resolve the time dependence of isotopic exchange between fluids and solid surfaces in reactive systems during net precipitation, and show that aspects of this problem are uniquely resolvable at the pore scale.

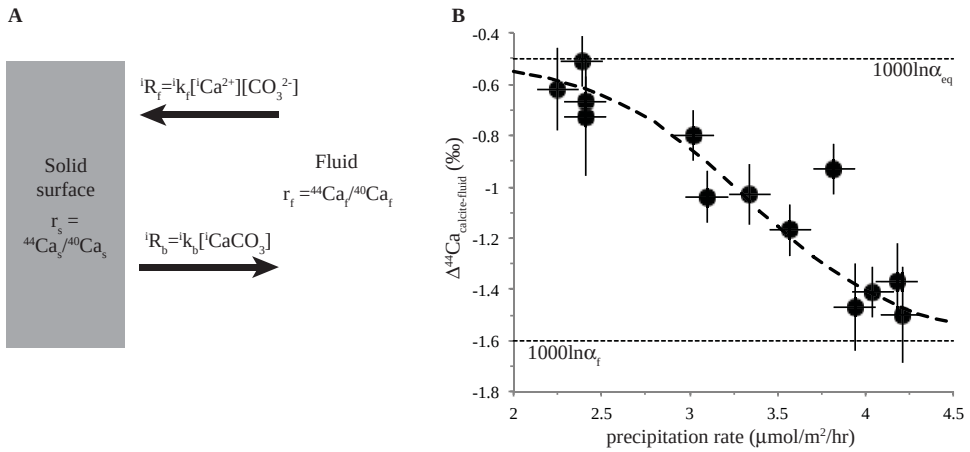

Figure 11. (A) schematic of the DePaolo (2011) model for calcium isotope fractionation during precipitation of calcite for a reversible reaction. (B) Application of the DePaolo (2011) model (heavy dashed line) to the Tang et al. (2008) dataset. The model is bounded between two values defined by α_f and α_{eq}.

TREATMENT OF TRANSIENT ISOTOPIC PARTITIONING AND ZONING

Extending the concept of a variable apparent fractionation factor to through-flowing, field scale systems has thus far been accomplished primarily through the use of continuum-scale reactive transport models. As discussed in the dissolution section, these models have commonly been applied to simulate fractionation during homogeneous (aqueous) reactions. Accumulation of a solid phase that is composed of two isotopes of the same element is problematic in that any change in the isotope ratio of the fluid through time needs to be incorporated into the solid phase without imposing an erroneous fractionation factor. Druhan et al. (2013) accommodated a variable solid phase isotopic composition in the context of calcium isotope partitioning during carbonate mineral precipitation using a solid solution. In common practice, the overall rate of carbonate mineral precipitation:

$$R_{net} = a_{CaCO_{3(s)}} k \left[\frac{a_{Ca^{2+}} a_{CO_3^{2-}}}{a_{CaCO_{3(s)}}} \frac{1}{K_{eq}} - 1 \right] \tag{30}$$

where k is the kinetic rate constant, K_{eq} is the equilibrium constant and a represents the activity of the individual species, is simplified by the fact that the activity of a pure solid phase is equal to unity ($a_{CaCO_{3(s)}} = 1$). In the Druhan et al. (2013) model, the isotopes of calcium are simulated as separate 'species', which are coupled through their precipitation rates as:

$${}^{40}R_{net} = a_{{}^{40}CaCO_{3(s)}} \, {}^{40}k \left[\frac{a_{{}^{40}Ca^{2+}} a_{CO_3^{2-}}}{a_{{}^{40}CaCO_{3(s)}}} \frac{1}{{}^{40}K_{eq}} - 1 \right] \tag{31a}$$

$${}^{44}R_{net} = a_{{}^{44}CaCO_{3(s)}} \, {}^{44}k \left[\frac{a_{{}^{44}Ca^{2+}} a_{CO_3^{2-}}}{a_{{}^{44}CaCO_{3(s)}}} \frac{1}{{}^{44}K_{eq}} - 1 \right] \tag{31b}$$

The key to this approach is the recognition that if $a_{CaCO_{3(s)}} = 1$, then the activities of the individual isotopologues of calcite must sum up to unity. Assuming an ideal solid solution,

these activities can be rewritten as mole fractions of the total mineral:

$$a_{^{40}\mathrm{CaCO_{3(s)}}} = X_{^{40}\mathrm{CaCO_{3(s)}}} = \frac{n_{^{40}\mathrm{CaCO_{3(s)}}}}{n_{^{40}\mathrm{CaCO_{3(s)}}} + n_{^{44}\mathrm{CaCO_{3(s)}}}} \tag{32a}$$

$$a_{^{44}\mathrm{CaCO_{3(s)}}} = X_{^{44}\mathrm{CaCO_{3(s)}}} = \frac{n_{^{44}\mathrm{CaCO_{3(s)}}}}{n_{^{40}\mathrm{CaCO_{3(s)}}} + n_{^{44}\mathrm{CaCO_{3(s)}}}} \tag{32b}$$

where n is the number of moles of each isotopologue of calcite. Expressing the mole fractions of the solid phase in the calculation of $^{40}R_{\mathrm{net}}$ and $^{44}R_{\mathrm{net}}$ effectively couples the two isotopes to one another in an overall expression for carbonate mineral accumulation as a solid solution model. The problem then becomes the definition of the mole fractions X. At one extreme, the back reaction between the solid phase and fluid may be suppressed by setting X equal to the instantaneous mole fraction of the isotopes in solution. This results in a system where the solid phase is isotopically segregated from the fluid, and the only mechanism of fractionation is through an irreversible α_k, that is the ratio of the kinetic rate constants. Such an approach would reproduce the isotopic dataset of the Skulan et al. (2002) hematite precipitation experiment (Fig. 9A). In systems where the back reaction is significant, the DePaolo (2011) conceptual framework would dictate that values of X represent the surface of the solid phase in contact with the surrounding fluid. In practice this value is not explicitly tracked in continuum scale models, which represent the composition of solid phases as volume fractions within a given discretized domain. Druhan et al. (2013) applied their model to a dataset of fluid calcium isotope ratios measured through time during unbuffered carbonate mineral precipitation. They noted that these data did not conform to a fixed fractionation factor through time (Fig. 12A), but an accurate simulation of the observed isotopic partitioning was obtained using Equations (31a,b) by approximating X as the isotopic composition of the bulk calcite as it accumulated through time (Fig. 12B).

Versions of this derivation in which isotopic fractionation was considered irreversible have been applied to chromium isotopes (Wanner et al. 2014) and sulfur isotopes (Druhan et al. 2014; Hubbard et al. 2014). Steefel et al. (2014a) described a variable fractionation factor for calcium isotopes in marine carbonates as a result of reversible reactivity using the same model, and provided a detailed derivation emphasizing the capacity to resolve isotopic re-equilibration unique to a model for the transient evolution of the coupled fluid and solid surface. Still, the accuracy of bulk-solid values of X presents a significant challenge because the composition of an isotopically distinct solid surface is homogenized with the preexisting solid over the volume of each gridblock. Druhan et al. (2013) and Steefel et al. (2014a) both provided approximations to the solid surface mole fractions by tracking a running average of the isotopic composition of material precipitating from solution as a function of time, resulting in an equally good representation of the measured fluid isotope ratios for a different value of α_k. Similarly, one may track the isotope composition of a distinct solid surface layer and allow for exchange/equilibration with that zone of the solid based on the mineral volume fraction, surface area and a representative length scale of each zone. However, as discussed in the dissolution section, this approach requires some independent, *a priori* knowledge of the length scales of zoning as well as tracking of the isotopic composition of multiple zones within the total volume of a solid.

A common theme emerging from the previous sections is that partitioning of isotopes across a phase boundary requires some parameterization of the isotopic composition of the solid surface and surrounding fluid distinct from 'bulk' or 'well mixed' reservoirs. The ability to describe isotopic partitioning unique to the phase boundary appears to influence the

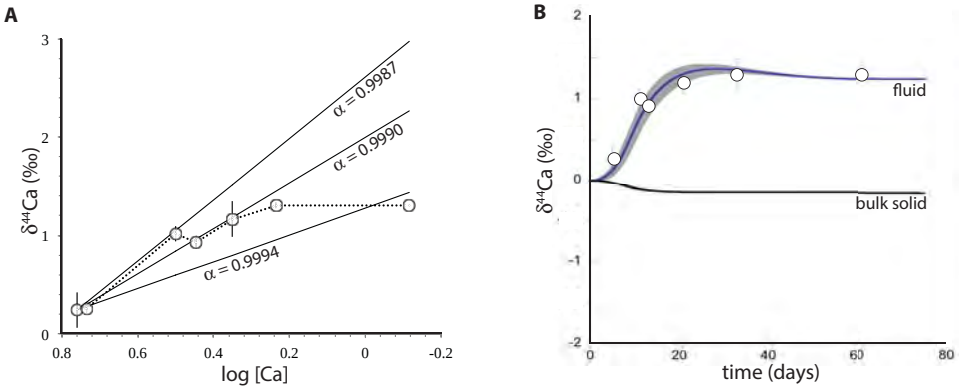

Figure 12. Fluid calcium isotope ratios and calcium concentrations measured as a function of time during unbuffered carbonate mineral precipitation. (A) Measured values (open circles) in comparison with Rayleigh models (solid lines) for three values of δ, showing that the data do not conform to a constant fractionation factor, modified from Druhan et al. (2013). (B) Reactive transport model of calcium isotope data as a function of time using Equations (32a,b), demonstrating good agreement with measured fluid values by approximating the mole fractions *X* with the bulk carbonate isotope composition. [Used with permission from Elsevier Limited, from Druhan JL, Steefel CI, Williams KH, DePaolo DJ (2013) Calcium isotope fractionation in groundwater: Molecular scale processes influencing field scale behavior. *Geochimica et Cosmoschimica Acta*, Vol. 119, Fig. 7A, p. 107.]

accuracy of simulations from highly variable, field scale systems (e.g., Druhan et al. 2013) to highly controlled laboratory experiments (e.g., Tang et al. 2008). This observation implies that .mechanistic descriptions of isotope partitioning could be significantly improved by modeling approaches that are capable of resolving spatial zoning both within a single phase and within individual crystals or grains (e.g., Li et al. 2006; Tartakovsky et al. 2008; Molins et al. 2012; Molins 2015, this volume; Yoon et al. 2015, this volume).

One such method is the use of a lattice Boltzmann approach (Yoon et al. 2015, this volume), which is capable of explicitly describing the location and shape of a boundary between independently discretized fluid and solid phases. This approach has previously been applied to describe heterogeneous reactivity (Kang et al. 2002, 2003, 2004) including multicomponent systems (Kang et al. 2006, 2007, 2010; Yoon et al. 2012). Recently, Huber et al. (2014) developed an approach to describe the transfer of mass across a phase boundary that is independent of the shape of the solid surface. This approach is well suited to the description of fractionating reactions that are coupled through isotope partitioning across a phase boundary. As a proof of concept, Figure 13 demonstrates application of the Huber et al. (2014) model to a closed system in which the fluid phase surrounding a grain of calcite is initially supersaturated with respect to the solid. Two isotopes of calcium are explicitly tracked using the formulations given in Equation (31a,b) over time as the system reaches chemical and isotopic equilibrium. Figure 13 depicts a particular snapshot in time, during which the fluid phase has not yet reached equilibrium with the solid. This disequilibrium is evident in the gradients of reactive species as well as the fluid isotope ratio with distance from the solid phase boundary. Importantly, the surface of the solid phase, which is composed of pure $CaCO_{3(s)}$ is also isotopically variable, and supplies a more accurate estimate of the values of the mole fraction for each isotope *X* (Eqn. 32) than previous bulk averaged estimates. This is not readily observed in the spatial distribution of isotope ratios because only a very small portion of the solid phase surface is considered in contact with the surrounding fluid. However, a time series plot of the isotope composition of the calcite surface clearly demonstrates this variability, which feeds back into the rate at which the fluid phase established isotopic equilibrium with the reactive solid surface.

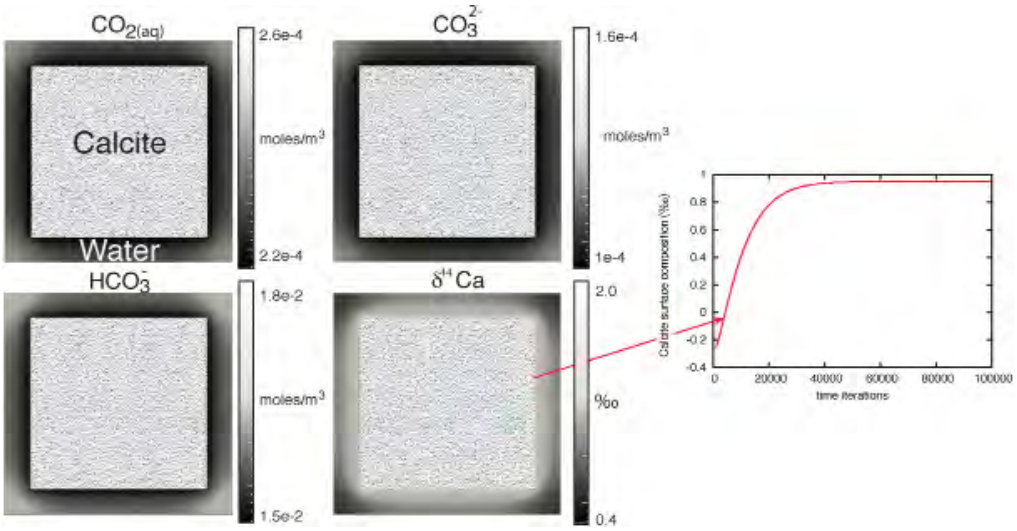

Figure 13. Lattice Boltzmann model of calcite precipitation based on the Huber et al. (2014) methodology, and including two isotopes of calcium using the modified TST rate laws of Druhan et al. (2013). A solid phase calcite grain (textured) is surrounded by a fluid phase that is initially supersaturated with respect to calcite. The domain is defined by no-flux boundary conditions. Spatial concentration and isotope ratios are shown for a given point in time during the transient approach to equilibrium. The isotopic composition of the solid surface in contact with the fluid is tracked, used to define *X* in Equation (32), and varies in tandem with the isotope ratio of the fluid through time.

This proof of concept exercise suggests that significant improvements could be gained from pore scale descriptions of isotopic partitioning during precipitation, dissolution, transport and decay. For example, application of the Druhan et al. (2013) derivation in a system where *X* (Eqn. 32) is only describable as the bulk solid phase value would fail to reproduce observed isotope partitioning during dissolution. The same is true for the closed form solutions of DePaolo (2011) and Brantley et al. (2004). The result is a situation in which reactions that generate isotope partitioning, which are formulated as a reversible departure from equilibrium, cannot be described across the range of saturation states from net dissolution to net precipitation with a single model. The use of pore scale discretization may provide a means of circumventing this discontinuity.

ACKNOWLEDGMENTS

This material is based in part upon work supported as part of the Subsurface Science Scientific Focus Area at Lawrence Berkeley National Laboratory funded by the U.S. Department of Energy, Office of Science, Office of Biological and Environmental Research and Office of Basic Earth Sciences, under Award Number DE-AC02-05CH11231. The authors wish to thank Kate Maher and Carl Steefel for their thoughtful comments, which greatly improved the chapter.

REFERENCES

Abe Y, Hunkeler D (2006) Does the Rayleigh equation apply to evaluate field isotope data in contaminant hydrogeology? Environ Sci Technol 40:1588–1596, doi:10.1021/es051128p

Aciego S, Bourdon B, Schwander J, Baur H, Forieri A (2011) Toward a radiometric ice clock: uranium ages of the Dome C ice core. Quaternary Science Reviews 30:2389–2397, doi:10.1016/j.quascirev.2011.06.008

Adloff JP, Roessler K (1991) Recoil and transmutation effects in the migration behavior of actinides. Radiochimic Acta 52-3:269–274, doi: 10.1524/ract.1991.5253.1.269

Beard BL, Johnson CM, Cox L, Sun H, Nealson KH, Aguilar C (1999) Iron isotope biosignatures. Science 285:1889–1892, doi:10.1126/science.285.5435.1889

Beard BL, Johnson CM, Skulan JL, Nealson KH, Cox L, Sun H (2003) Application of Fe isotopes to tracing the geochemical and biological cycling of Fe. Chem Geol 195:87–117, doi:10.1016/s0009-2541(02)00390-x

Bellin A, Tonina D (2007) Probability density function of non-reactive solute concentration in heterogeneous porous formations. J Contam Hydrol 94:109–125, doi:10.1016/j.jconhyd.2007.05.005

Berna EC, Johnson TM, Makdisi RS, Basui A (2010) Cr stable isotopes as indicators of Cr(VI) reduction in groundwater: A detailed time-series study of a point-source plume. Environ Sci Technol 44:1043–1048, doi:10.1021/es902280s

Bourdon B, Bureau S, Andersen MB, Pili E, Hubert A (2009) Weathering rates from top to bottom in a carbonate environment. Chem Geol 258:275–287, doi:10.1016/j.chemgeo.2008.10.026

Bourg IC, Sposito G (2007) Modeling cation diffusion in compacted water-saturated sodium bentonite at low ionic strength. Environ Sci Technol 41:8118–8122, doi:10.1021/es0717212

Bourg IC, Richter FM, Christensen JN, Sposito G (2010) Isotopic mass dependence of metal cation diffusion coefficients in liquid water. Geochim Cosmochim Acta 74:2249–2256, doi:10.1016/j.gca.2010.01.024

Bracco JN, Stack AG, Steefel CI (2013) Upscaling calcite growth rates from the mesoscale to the macroscale. Environ Sci Technol 47:7555–7562, doi:10.1021/es400687r

Brandes JA, Devol AH (1997) Isotopic fractionation of oxygen and nitrogen in coastal marine sediments. Geochim Cosmochim Acta 61:1793–1801, doi:10.1016/s0016-7037(97)00041-0

Brantley SL, Liermann L, Bullen TD (2001) Fractionation of Fe isotopes by soil microbes and organic acids. Geology 29:535–538, doi:10.1130/0091-7613(2001)029<0535:fofibs>2.0.co;2

Brantley SL, Liermann LJ, Guynn RL, Anbar A, Icopini GA, Barling J (2004) Fe isotopic fractionation during mineral dissolution with and without bacteria. Geochim Cosmochim Acta 68:3189–3204, doi:10.1016/j.gca.2004.01.023

Casey WH, Ludwig C (1996) The mechanism of dissolution of oxide minerals. Nature 381:506–509, doi:10.1038/381506a0

Casey WH, Westrich HR, Banfield JF, Ferruzzi G, Arnold GW (1993) Leaching and reconstruction at the surfaces of dissolving chain-silicate minerals. Nature 366:253–256, doi:10.1038/366253a0

Chacko T, Cole DR, Horita J (2001) Equilibrium oxygen, hydrogen and carbon isotope fractionation factors applicable to geologic systems. Rev Mineral Geochem 43:1–81, doi:10.2138/gsrmg.43.1.1

Chalov PI (1959) The U^{234}/U^{238} ratio in some secondary minerals. Geochem 2:203-210

Chapman JB, Weiss DJ, Shan Y, Lemburger M (2009) Iron isotope fractionation during leaching of granite and basalt by hydrochloric and oxalic acids. Geochim Cosmochim Acta 73:1312–1324, doi:10.1016/j.gca.2008.11.037

Chou L, Garrels RM, Wollast R (1989) Comparative-study of the kinetics and mechanisms of dissolution of carbonate minerals. Chem Geol 78:269–282, doi:10.1016/0009-2541(89)90063-6

Clark SK, Johnson TM (2008) Effective isotopic fractionation factors for solute removal by reactive sediments: a laboratory microcosm and slurry study. Environ Sci Technol 42:7850–7855, doi:10.1021/es801814v

Coplen TB (2011) Guidelines and recommended terms for expression of stable-isotope-ratio and gas-ratio measurement results. Rapid Commun Mass Spectrom 25:2538–2560, doi:10.1002/rcm.5129

Criss RE (1999) Principles of Stable Isotope Distribution. Oxford University Press

Crosby HA, Roden EE, Johnson CM, Beard BL (2007) The mechanisms of iron isotope fractionation produced during dissimilatory Fe(III) reduction by *Shewanella putrefaciens* and *Geobacter sulfurreducens*. Geobiol 5:169–189, doi:10.1111/j.1472-4669.2007.00103.x

Dale AW, Bruchert V, Alperin M, Regnier P (2009) An integrated sulfur isotope model for Namibian shelf sediments. Geochim Cosmochim Acta 73:1924–1944, doi:10.1016/j.gca.2008.12.015

Dellinger M, Gaillardet J, Bouchez J, Calmels D, Galy V, Hilton RG, Louvat P, France-Lanord C (2014) Lithium isotopes in large rivers reveal the cannibalistic nature of modern continental weathering and erosion. Earth Planet Sci Lett 401:359–372, doi:10.1016/j.epsl.2014.05.061

DePaolo DJ (2011) Surface kinetic model for isotopic and trace element fractionation during precipitation of calcite from aqueous solutions. Geochim Cosmochim Acta 75:1039–1056, doi:10.1016/j.gca.2010.11.020

DePaolo DJ, Maher K, Christensen JN, McManus J (2006) Sediment transport time measured with U-series isotopes: Results from ODP North Atlantic drift site 984. Earth Planet Sci Lett 248:394–410, doi:10.1016/j.epsl.2006.06.004

DePaolo DJ, Lee VE, Christensen JN, Maher K (2012) Uranium comminution ages: Sediment transport and deposition time scales. C R Geosci 344:678–687, doi:10.1016/j.crte.2012.10.014

Dietzel M, Tang J, Leis A, Koehler SJ (2009) Oxygen isotopic fractionation during inorganic calcite precipitation - Effects of temperature, precipitation rate and pH. Chem Geol 268:107–115, doi:10.1016/j.chemgeo.2009.07.015

Dosseto A, Turner SP, Douglas GB (2006) Uranium-series isotopes in colloids and suspended sediments: Timescale for sediment production and transport in the Murray-Darling River system. Earth Planet Sci Lett 246:418–431, doi:10.1016/j.epsl.2006.04.019

Druhan JL, Steefel CI, Molins S, Williams KH, Conrad ME, DePaolo DJ (2012) Timing the Onset of Sulfate Reduction over Multiple Subsurface Acetate Amendments by Measurement and Modeling of Sulfur Isotope Fractionation. Environ Sci Technol 46:8895-8902, doi:10.1021/es302016p

Druhan JL, Steefel CI, Williams KH, DePaolo DJ (2013) Calcium isotope fractionation in groundwater: Molecular scale processes influencing field scale behavior. Geochim Cosmochim Acta 119:93–116, doi:10.1016/j.gca.2013.05.022

Druhan JL, Steefel CI, Conrad ME, DePaolo DJ (2014) A large column analog experiment of stable isotope variations during reactive transport: I. A comprehensive model of sulfur cycling and delta S-34 fractionation. Geochim Cosmochim Acta 124:366–393, doi:10.1016/j.gca.2013.08.037

Eckert D, Rolle M, Cirpka OA (2012) Numerical simulation of isotope fractionation in steady-state bioreactive transport controlled by transverse mixing. J Contam Hydrol 140:95–106, doi:10.1016/j.jconhyd.2012.08.010

Eggenkamp HGM, Coleman ML (2009) The effect of aqueous diffusion on the fractionation of chlorine and bromine stable isotopes. Geochim Cosmochim Acta 73:3539–3548, doi:10.1016/j.gca.2009.03.036

Eiler JM (2007) "Clumped-isotope" geochemistry - The study of naturally-occurring, multiply-substituted isotopologues. Earth Planet Sci Lett 262:309–327, doi:10.1016/j.epsl.2007.08.020

Epstein S, Mayeda T (1953) Variation of O-18 content of waters from natural sources. Geochim Cosmochim Acta 4:213–224, doi:10.1016/0016-7037(53)90051-9

Fantle MS, DePaolo DJ (2007) Ca isotopes in carbonate sediment and pore fluid from ODP Site 807A: The Ca2+(aq)-calcite equilibrium fractionation factor and calcite recrystallization rates in Pleistocene sediments. Geochim Cosmochim Acta 71:2524–2546, doi:10.1016/j.gca.2007.03.006

Fantle MS, Tipper ET (2014) Calcium isotopes in the global biogeochemical Ca cycle: Implications for development of a Ca isotope proxy. Earth-Sci Rev 129:148–177, doi:10.1016/j.earscirev.2013.10.004

Fernandez A, Borrok DM (2009) Fractionation of Cu, Fe, and Zn isotopes during the oxidative weathering of sulfide-rich rocks. Chem Geol 264:1–12, doi:10.1016/j.chemgeo.2009.01.024

Fleischer RL (1980) Isotopic disequilibrium of Uranium - alpha-recoil damage and preferential solution effects. Science 207:979–981, doi:10.1126/science.207.4434.979

Fleischer RL (1988) Alpha-recoil damage - relation to isotopic disequilibrium and leaching of radionuclides. Geochim Cosmochim Acta 52:1459–1466, doi:10.1016/0016-7037(88)90216-5

Fleischer RL, Raabe OG (1978) Recoiling alpha-emitting nuclei – mechanisms for uranium-series disequilibrium. Geochim Cosmochim Acta 42:973–978, doi:10.1016/0016-7037(78)90286-7

Gabitov RI (2013) Growth-rate induced disequilibrium of oxygen isotopes in aragonite: An in situ study. Chem Geol 351:268–275, doi:10.1016/j.chemgeo.2013.05.015

Gabitov RI, Watson EB, Sadekov A (2012) Oxygen isotope fractionation between calcite and fluid as a function of growth rate and temperature: An in situ study. Chem Geol 306:92–102, doi:10.1016/j.chemgeo.2012.02.021

Galy A, Bar-Matthews M, Halicz L, O'Nions RK (2002) Mg isotopic composition of carbonate: insight from speleothem formation. Earth Planet Sci Lett 201:105–115, doi:10.1016/s0012-821x(02)00675-1

Geilert S, Vroon PZ, Roerdink DL, Van Cappellen P, van Bergen MJ (2014) Silicon isotope fractionation during abiotic silica precipitation at low temperatures: Inferences from flow-through experiments. Geochim Cosmochim Acta 142:95–114, doi:10.1016/j.gca.2014.07.003

Gelhar LW, Axness CL (1983) 3-dimensional stochastic-analysis of macrodispersion in aquifers. Water Resour Res 19:161–180, doi:10.1029/WR019i001p00161

Georg RB, Reynolds BC, Frank M, Halliday AN (2006) Mechanisms controlling the silicon isotopic compositions of river waters. Earth Planet Sci Lett 249:290–306, doi:10.1016/j.epsl.2006.07.006

Georg RB, Reynolds BC, West AJ, Burton KW, Halliday AN (2007) Silicon isotope variations accompanying basalt weathering in Iceland. Earth Planet Sci Lett 261:476–490, doi:10.1016/j.epsl.2007.07.004

Gibson BD, Amos RT, Blowes DW (2011) S-34/S-32 Fractionation during Sulfate Reduction in Groundwater Treatment Systems: Reactive Transport Modeling. Environ Sci Technol 45:2863–2870, doi:10.1021/es1038276

Gussone N, Bohm F, Eisenhauer A, Dietzel M, Heuser A, Teichert BMA, Reitner J, Worheide G, Dullo WC (2005) Calcium isotope fractionation in calcite and aragonite. Geochim Cosmochim Acta 69:4485–4494, doi:10.1016/j.gca.2005.06.003

Handley HK, Turner S, Afonso JC, Dosseto A, Cohen T (2013) Sediment residence times constrained by uranium-series isotopes: A critical appraisal of the comminution approach. Geochim Cosmochim Acta 103:245–262, doi:10.1016/j.gca.2012.10.047

Helgeson HC, Murphy WM, Aagaard P (1984) Thermodynamic and kinetic constraints on reaction-rates among minerals and aqueous-solutions: 2. Rate constants, effective surface-area, and the hydrolysis of feldspar. Geochim Cosmochim Acta 48:2405–2432, doi:10.1016/0016-7037(84)90294-1

Hellmann R, Eggleston CM, Hochella MF, Crerar DA (1990) The formation of leached layers on albite surfaces during dissolution under hydrothermal conditions. Geochim Cosmochim Acta 54:1267–1281, doi:10.1016/0016-7037(90)90152-b

Hellmann R, Wirth R, Daval D, Barnes J-P, Penisson J-M, Tisserand D, Epicier T, Florin B, Hervig RL (2012) Unifying natural and laboratory chemical weathering with interfacial dissolution-reprecipitation: A study based on the nanometer-scale chemistry of fluid–silicate interfaces. Chem Geol 294:203–216, doi:10.1016/j.chemgeo.2011.12.002

Hellmann R, Cotte S, Cadel E, Malladi S, Karlsson LS, Lozano-Perez S, Cabie M, Seyeux A (2015) Nanometre-scale evidence for interfacial dissolution–reprecipitation control of silicate glass corrosion. Nat Mater 14:307–311, doi: 10.1038/nmat4172

Henderson GM, Slowey NC, Fleisher MQ (2001) U-Th dating of carbonate platform and slope sediments. Geochim Cosmochim Acta 65:2757–2770, doi:10.1016/s0016-7037(01)00621-4

Hochstetler DL, Rolle M, Chiogna G, Haberer CM, Grathwohl P, Kitanidis PK (2013) Effects of compound-specific transverse mixing on steady-state reactive plumes: Insights from pore-scale simulations and Darcy-scale experiments. Adv Water Resour 54:1–10, doi:10.1016/j.advwatres.2012.12.007

Hofmann AE, Bourg IC, DePaolo DJ (2012) Ion desolvation as a mechanism for kinetic isotope fractionation in aqueous systems. PNAS 109:18689–18694, doi:10.1073/pnas.1208184109

Hubbard CG, Cheng Y, Engelbrekston A, Druhan JL, Li L, Ajo-Franklin JB, Coates JD, Conrad ME (2014) Isotopic insights into microbial sulfur cycling in oil reservoirs. Front Microbiol 5:480, doi:10.3389/fmicb.2014.00480

Huber C, Shafei B, Parmigiani A (2014) A new pore-scale model for linear and non-linear heterogeneous dissolution and precipitation. Geochim Cosmochim Acta 124:109–130, doi:10.1016/j.gca.2013.09.003

Immenhauser A, Buhl D, Richter D, Niedermayr A, Riechelmann D, Dietzel M, Schulte U (2010) Magnesium-isotope fractionation during low-Mg calcite precipitation in a limestone cave - Field study and experiments. Geochim Cosmochim Acta 74:4346–4364, doi:10.1016/j.gca.2010.05.006

Jacobson AD, Holmden C (2008) delta(44)Ca evolution in a carbonate aquifer and its bearing on the equilibrium isotope fractionation factor for calcite. Earth Planet Sci Lett 270:349–353, doi:10.1016/j.epsl.2008.03.039

Jamieson-Hanes JH, Amos RT, Blowes DW (2012) Reactive Transport Modeling of Chromium Isotope Fractionation during Cr(VI) Reduction. Environ Sci Technol 46:13311–13316, doi:10.1021/es3046235

Johnson TM (2011) Stable Isotopes of Cr and Se as Tracers of Redox Processes in Earth Surface Environments. *In:* Handbook of Environmental Isotope Geochemistry, Vol. 1 & 2, M Baskaran (ed) Springer-Verlag, Berlin, p 155-176, doi: 10.1007/978-3-642-10637-8

Johnson CM, Beard BL, Albarede F (2004) Overview and general concepts. Rev Mineral Geochem 55:1-24, doi 10.2138/gsrmg.55.1.1

Kang Q, Zhang DX, Chen SY, He XY (2002) Lattice Boltzmann simulation of chemical dissolution in porous media. Phys Rev E 65:036318, doi:10.1103/PhysRevE.65.036318

Kang Q, Zhang DX, Chen SY (2003) Simulation of dissolution and precipitation in porous media. J Geophys Res-Solid Earth 108(B10):2505, doi:10.1029/2003jb002504

Kang Q, Zhang DX, Lichtner PC, Tsimpanogiannis IN (2004) Lattice Boltzmann model for crystal growth from supersaturated solution. Geophysical Research Letters 31:L21604, doi:10.1029/2004gl021107

Kang Q, Lichtner PC, Zhang D (2006) Lattice Boltzmann pore-scale model for multicomponent reactive transport in porous media. J Geophys Res-Solid Earth 111:B05203, doi:10.1029/2005jb003951

Kang Q, Lichtner PC, Zhang D (2007) An improved lattice Boltzmann model for multicomponent reactive transport in porous media at the pore scale. Water Resour Res 43:W12S14, doi:10.1029/2006wr005551

Kang Q, Lichtner PC, Viswanathan HS, Abdel-Fattah AI (2010) Pore scale modeling of reactive transport involved in geologic CO_2 sequestration. Transport Porous Med 82:197–213, doi:10.1007/s11242-009-9443-9

Kaufman S, Libby WF (1954) The natural distribution of tritium. Physical Review 93:1337–1344, doi:10.1103/PhysRev.93.1337

Kiczka M, Wiederhold JG, Frommer J, Kraemer SM, Bourdon B, Kretzschmar R (2010) Iron isotope fractionation during proton- and ligand-promoted dissolution of primary phyllosilicates. Geochim Cosmochim Acta 74:3112–3128, doi:10.1016/j.gca.2010.02.018

Kigoshi K (1971) Alpha-recoil thorium-234-dissolution into water and uranium-234/uranium-238 disequilibrium in nature. Science 173:47-48, doi:10.1126/science.173.3991.47

Kim ST, Oneil JR (1997) Equilibrium and nonequilibrium oxygen isotope effects in synthetic carbonates. Geochim Cosmochim Acta 61:3461–3475, doi:10.1016/s0016-7037(97)00169-5

Kisakuerek B, Niedermayr A, Mueller MN, Taubner I, Eisenhauer A, Dietzel M, Buhl D, Fietzke J, Erez J (2009) Magnesium isotope fractionation in inorganic and biogenic calcite. Geochim Cosmochim Acta 73:A663–A663

Kolodny Y, Kaplan IR (1970) Uranium isotopes in sea-floor phosphorites. Geochim Cosmochim Acta 34:3–24, doi:10.1016/0016-7037(70)90148-1

Krane KS (1988) Introductory Nuclear Physics 3rd Ed. Wiley

Ku TL, Luo S, Leslie BW, Hammond DE (1992) Decay-series disequilibria applied to the study of rock–water interaction and geothermal systems. *In:* Uranium-series Disequilibrium: Applications to Earth, Marine and Environmental Sciences, 2nd ed. (M Ivanovich and RS Harmon, eds), Clarendon Press, Oxford, p 631–668.

Kump LR, Brantley SL, Arthur MA (2000) Chemical, weathering, atmospheric CO_2, and climate. Ann Rev Earth Planet Sci 28:611–667, doi:10.1146/annurev.earth.28.1.611

Kunze RW, Fuoss RM (1962) Conductance of alkali halides: III. The Isotopic lithium chlorides. J Phys Chem 66:930-931, doi:10.1021/j100811a043

LaBolle EM, Fogg GE, Eweis JB, Gravner J, Leaist DG (2008) Isotopic fractionation by diffusion in groundwater. Water Resour Res 44:W07405, doi:10.1029/2006wr005264

Lee VE, DePaolo DJ, Christensen JN (2010) Uranium-series comminution ages of continental sediments: Case study of a Pleistocene alluvial fan. Earth Planet Sci Lett 296:244–254, doi:10.1016/j.epsl.2010.05.005

Lemarchand D, Wasserburg GT, Papanastassiou DA (2004) Rate-controlled calcium isotope fractionation in synthetic calcite. Geochim Cosmochim Acta 68:4665–4678, doi:10.1016/j.gca.2004.05.029

Lemarchand E, Chabaux F, Vigier N, Millot R, Pierret M-C (2010) Lithium isotope systematics in a forested granitic catchment (Strengbach, Vosges Mountains, France). Geochim Cosmochim Acta 74:4612–4628, doi:10.1016/j.gca.2010.04.057

Li L, Peters CA, Celia MA (2006) Upscaling geochemical reaction rates using pore-scale network modeling. Adv Water Resour 29:1351–1370, doi:10.1016/j.advwatres.2005.10.011

Li L, Steefel CI, Kowalsky MB, Englert A, Hubbard SS (2010) Effects of physical and geochemical heterogeneities on mineral transformation and biomass accumulation during biostimulation experiments at Rifle, Colorado. J Contam Hydrol 112:45–63, doi:10.1016/j.jconhyd.2009.10.006

Li L, Salehikhoo F, Brantley SL, Heidari P (2014) Spatial zonation limits magnesite dissolution in porous media. Geochim Cosmochim Acta 126:555–573, doi:10.1016/j.gca.2013.10.051

Maher K (2010) The dependence of chemical weathering rates on fluid residence time. Earth Planet Sci Lett 294:101–110, doi:10.1016/j.epsl.2010.03.010

Maher K (2011) The role of fluid residence time and topographic scales in determining chemical fluxes from landscapes. Earth Planet Sci Lett 312:48–58, doi:10.1016/j.epsl.2011.09.040

Maher K, Chamberlain CP (2014) Hydrologic regulation of chemical weathering and the geologic carbon cycle. Science 343:1502–1504, doi:10.1126/science.1250770

Maher K, DePaolo DJ, Lin JCF (2004) Rates of silicate dissolution in deep-sea sediment: In situ measurement using U-234/U-238 of pore fluids. Geochim Cosmochim Acta 68:4629–4648, doi:10.1016/j.gca.2004.04.024

Maher K, DePaolo DJ, Christensen JN (2006a) U-Sr isotopic speedometer: Fluid flow and chemical weathering rates in aquifers. Geochim Cosmochim Acta 70:4417–4435, doi:10.1016/j.gca.2006.06.1559

Maher K, Steefel CI, DePaolo DJ, Viani BE (2006b) The mineral dissolution rate conundrum: Insights from reactive transport modeling of U isotopes and pore fluid chemistry in marine sediments. Geochim Cosmochim Acta 70:337–363, doi:10.1016/j.gca.2005.09.001

Malmstrom ME, Destouni G, Banwart SA, Stromberg BHE (2000) Resolving the scale-dependence of mineral weathering rates. Environ Sci Technol 34:1375–1378, doi:10.1021/es990682u

Maloszewski P, Zuber A (1982) Determining the turnover time of groundwater systems with the aid of environmental tracers: 1. Models and their applicability. J Hydrol 57:207–231, doi: 10.1016/0022-1694(82)90147-0

Marriott CS, Henderson GM, Belshaw NS, Tudhope AW (2004) Temperature dependence of delta Li-7, delta Ca-44 and Li/Ca during growth of calcium carbonate. Earth Planet Sci Lett 222:615–624, doi:10.1016/j.epsl.2004.02.031

Mariotti A, Germon JC, Hubert P, Kaiser P, Letolle R, Tardieux A, Tardieux P (1981) Experimental-determination of nitrogen kinetic isotope fractionation - some principles - illustration for the denitrification and nitrification processes. Plant and Soil 62:413–430, doi:10.1007/bf02374138

Mathur R, Ruiz J, Titley S, Liermann L, Buss H, Brantley S (2005) Cu isotopic fractionation in the supergene environment with and without bacteria. Geochim Cosmochim Acta 69:5233–5246, doi:10.1016/j.gca.2005.06.022

Mavromatis V, Gautier Q, Bosc O, Schott J (2013) Kinetics of Mg partition and Mg stable isotope fractionation during its incorporation in calcite. Geochim Cosmochim Acta 114:188–203, doi:10.1016/j.gca.2013.03.024

Meheut M, Lazzeri M, Balan E, Mauri F (2007) Equilibrium isotopic fractionation in the kaolinite, quartz, water system: Prediction from first-principles density-functional theory. Geochim Cosmochim Acta 71:3170–3181, doi:10.1016/j.gca.2007.04.012

Meheut M, Lazzeri M, Balan E, Mauri F (2009) Structural control over equilibrium silicon and oxygen isotopic fractionation: A first-principles density-functional theory study. Chem Geol 258:28–37, doi:10.1016/j.chemgeo.2008.06.051

Mickler PJ, Stern LA, Banner JL (2006) Large kinetic isotope effects in modern speleothems. Geol Soc Am Bull 118:65–81, doi:10.1130/b25698.1

Millot R, Vigier N, Gaillardet J (2010) Behaviour of lithium and its isotopes during weathering in the Mackenzie Basin, Canada. Geochim Cosmochim Acta 74:3897–3912, doi:10.1016/j.gca.2010.04.025

Molins S (2015) Reactive interfaces in direct numerical simulation of pore scale processes. Rev Mineral Geochem 80:461–481

Molins S, Trebotich D, Steefel CI, Shen C (2012) An investigation of the effect of pore scale flow on average geochemical reaction rates using direct numerical simulation. Water Resour Res 48:W03527, doi:10.1029/2011wr011404

Moller KB, Rey R, Masia M, Hynes JT (2005) On the coupling between molecular diffusion and solvation shell exchange. J Chem Phys 122:114508, doi:10.1063/1.1863172

Moore WS (1976) Sampling Ra-228 in deep ocean. Deep-Sea Res 23:647–651, doi:10.1016/0011-7471(76)90007-3

Nielsen LC, DePaolo DJ, De Yoreo JJ (2012) Self-consistent ion-by-ion growth model for kinetic isotopic fractionation during calcite precipitation. Geochim Cosmochim Acta 86:166–181, doi:10.1016/j.gca.2012.02.009

Oelkers EH (2001) General kinetic description of multioxide silicate mineral and glass dissolution. Geochim Cosmochim Acta 65:3703–3719, doi:10.1016/s0016-7037(01)00710-4

Oelze M, von Blanckenberg F, Bouchez J, Hoellen D, Dietzel M (2015) The effects of Al on Si isotope fractionation investigated by silica precipitation experiments. Chem Geol 397:94–105, doi:10.1016/j.chemgeo.2015.01.002

Opfergelt S, Burton KW, Pogge von Strandmann PAE, Gislason SR, Halliday AN (2013) Riverine silicon isotope variations in glaciated basaltic terrains: Implications for the Si delivery to the ocean over glacial-interglacial intervals. Earth Planet Sci Lett 369:211–219, doi:10.1016/j.epsl.2013.03.025

Oster JL, Ibarra DE, Harris CR, Maher K (2012) Influence of eolian deposition and rainfall amounts on the U-isotopic composition of soil water and soil minerals. Geochim Cosmochim Acta 88:146–166, doi:10.1016/j.gca.2012.04.004

Pearce CR, Saldi GD, Schott J, Oelkers EH (2012) Isotopic fractionation during congruent dissolution, precipitation and at equilibrium: Evidence from Mg isotopes. Geochim Cosmochim Acta 92:170–183, doi:10.1016/j.gca.2012.05.045

Porcelli D, Baskaran M (2011) An overview of isotope geochemistry in environmental studies. In: Handbook of Environmental Isotope Geochemistry, Vol. 1 & 2, M Baskaran (ed) Springer-Verlag, Berlin, p 11–32, doi:10.1007/978-3-642-10637-8

Porcelli D, Swarzenski PW (2003) The behavior of U- and Th-series nuclides in groundwater. Rev Mineral Geochem 52:317–361, doi:10.2113/0520317

Porcelli D, Andersson PS, Wasserburg GJ, Ingri J, Baskaran M (1997) The importance of colloids and mires for the transport of uranium isotopes through the Kalix River watershed and Baltic Sea. Geochim Cosmochim Acta 61:4095–4113, doi:10.1016/s0016-7037(97)00235-4

Rasouli P, Steefel CI, Mayer KU, Rolle M (2015) Benchmarks for multicomponent diffusion and electrochemical migration. Comput Geosci, doi:10.1007/s10596-015-9481-z

Rayleigh L (1902) On the distillation of binary mixtures. Phil Mag 4:521–537

Regil EO, Schleiffer JJ, Adloff JP, Roessler K (1989) Chemical effects of alpha-decay in uranium minerals. Radiochimica Acta 47:177–185

Reynard LM, Day CC, Henderson GM (2011) Large fractionation of calcium isotopes during cave-analogue calcium carbonate growth. Geochim Cosmochim Acta 75:3726–3740, doi:10.1016/j.gca.2011.04.010

Richter FM, Mendybaev RA, Christensen JN, Hutcheon ID, Williams RW, Sturchio NC, Beloso AD (2006) Kinetic isotopic fractionation during diffusion of ionic species in water. Geochim Cosmochim Acta 70:277–289, doi:10.1016/j.gca.2005.09.016

Roessler K (1983) Uranium recoil reactions. *In*: Uranium Supplement: Handbook of Inorganic Chemistry. Vol A6. KC Buschbeck, C Keller (eds) Springer-Verlag, Berlin, p 135–164

Roessler K (1989) Thorium recoil reactions. *In*: Thorium Supplement: Handbook of Inorganic Chemistry. Vol A4. R Keim, C Keller (eds) Springer-Verlag, Berlin, p 199–246

Rolle M, Eberhardt C, Chiogna G, Cirpka OA, Grathwohl P (2009) Enhancement of dilution and transverse reactive mixing in porous media: Experiments and model-based interpretation. J Contam Hydrol 110:130–142, doi:10.1016/j.jconhyd.2009.10.003

Romanek CS, Grossman EL, Morse JW (1992) Carbon isotopic fractionation in synthetic aragonite and calcite - effects of temperature and precipitation rate. Geochim Cosmochim Acta 56:419–430, doi:10.1016/0016-7037(92)90142-6

Rosholt JN, Shields WR, Garner EL (1963) Isotopic fractionation of uranium in sandstone. Science 139:224-226, doi:10.1126/science.139.3551.224

Rustad JR, Casey WH, Yin Q-Z, Bylaska EJ, Felmy AR, Bogatko SA, Jackson VE, Dixon DA (2010) Isotopic fractionation of Mg2+(aq), Ca2+(aq), and Fe2+(aq) with carbonate minerals. Geochim Cosmochim Acta 74:6301–6323, doi:10.1016/j.gca.2010.08.018

Ryu J-S, Jacobson AD, Holmden C, Lundstrom C, Zhang Z (2011) The major ion, delta Ca-44/40, delta Ca-44/42, and delta Mg-26/24 geochemistry of granite weathering at pH=1 and T=25 degrees C: power-law processes and the relative reactivity of minerals. Geochim Cosmochim Acta 75:6004–6026, doi:10.1016/j.gca.2011.07.025

Schauble EA (2004) Applying stable isotope fractionation theory to new systems. Rev Mineral Geochem 55:65–111, doi 10.2138/gsrmg.55.1.65

Semkow TM (1990) Recoil-emanation theory applied to radon release from mineral grains. Geochim Cosmochim Acta 54:425–440, doi:10.1016/0016-7037(90)90331-e

Skulan JL, Beard BL, Johnson CM (2002) Kinetic and equilibrium Fe isotope fractionation between aqueous Fe(III) and hematite. Geochim Cosmochim Acta 66:2995–3015, doi:10.1016/s0016-7037(02)00902-x

Stack AG (2014) Next generation models of carbonate mineral growth and dissolution. Greenhouse Gas-Sci Technol 4:278–288, doi:10.1002/ghg.1400

Steefel CI, Lichtner PC (1998) Multicomponent reactive transport in discrete fractures: I. Controls on reaction front geometry. J Hydrol 209:186–199, doi:10.1016/s0022-1694(98)00146-2

Steefel CI, Maher K (2009) Fluid–rock interaction: a reactive transport approach. Rev Mineral Geochem 70:485–532, doi 10.2138/rmg.2009.70.11

Steefel CI, Molins S, Trebotich D (2013) Pore scale processes associated with subsurface CO_2 injection and sequestration. Rev Mineral Geochem 77:259–303, doi: 10.2138/rmg.2013.77.8

Steefel CI, Druhan JL, Maher K (2014a) Modeling coupled chemical and isotopic equilibration rates. Proc Earth Planet Sci 10:208–217, doi:10.1016/j.proeps.2014.08.022

Steefel CI, Appelo CAJ, Arora B, Jacques D, Kalbacher T, Kolditz O, Lagneau V, Lichtner PC, Mayer KU, Meeussen JCL, Molins S, Moulton D, Shao H, Šimůnek J, Spycher N, Yabusaki SB, Yeh GT (2015) Reactive transport codes for subsurface environmental simulation. Comput Geosci, doi:10.1007/s10569-014-9443-x

Sudicky EA, Illman WA, Goltz IK, Adams JJ, McLaren RG (2010) Heterogeneity in hydraulic conductivity and its role on the macroscale transport of a solute plume: From measurements to a practical application of stochastic flow and transport theory. Water Resour Res 46:W01508, doi:10.1029/2008wr007558

Sun HB, Semkow TM (1998) Mobilization of thorium, radium and radon radionuclides in ground water by successive alpha-recoils. J Hydrol 205:126–136, doi:10.1016/s0022-1694(97)00154-6

Tang J, Dietzel M, Boehm F, Koehler SJ, Eisenhauer A (2008) Sr2+/Ca2+ and Ca-44/Ca-40 fractionation during inorganic calcite formation: II. Ca isotopes. Geochim Cosmochim Acta 72:3733–3745, doi:10.1016/j.gca.2008.05.033

Tartakovsky AM, Redden G, Lichtner PC, Scheibe TD, Meakin P (2008) Mixing-induced precipitation: Experimental study and multiscale numerical analysis. Water Resour Res 44:W06S04, doi:10.1029/2006wr005725

Tipper ET, Calmels D, Gaillardet J, Louvat P, Capmas F, Dubacq B (2012) Positive correlation between Li and Mg isotope ratios in the river waters of the Mackenzie Basin challenges the interpretation of apparent isotopic fractionation during weathering. Earth Planet Sci Lett 333:35–45, doi:10.1016/j.epsl.2012.04.023

Torgersen T (1980) Controls on pore-fluid concentration of He-4 and Rn-222 and the calculation of He-4-Rn-222 ages. J Geochem Explor 13:57–75, doi:10.1016/0375-6742(80)90021-7

Tournassat C, Steefel CI (2015) Ionic transport in nano-porous clays with consideration of electrostatic effects. Rev Mineral Geochem 80:287–329

Tricca A, Wasserburg GJ, Porcelli D, Baskaran M (2001) The transport of U- and Th-series nuclides in a sandy unconfined aquifer. Geochim Cosmochim Acta 65:1187–1210, doi:10.1016/s0016-7037(00)00617-7

Turkowsky C (1969) Electron-microscopic observation of artificially produced alpha-recoil tracks in albite. Earth Planet Sci Lett 5:492–496, doi: 10.1016/S0012-821X(68)80084-6

Urey HC (1947) The thermodynamic properties of isotopic substances. J Chem Soc:562–581, doi:10.1039/jr9470000562

Van Breukelen BM (2007) Extending the Rayleigh equation to allow competing isotope fractionating pathways to improve quantification of biodegradation. Environ Sci Technol 41:4004–4010, doi:10.1021/es0628452

Van Breukelen BM, Prommer H (2008) Beyond the Rayleigh equation: Reactive transport modeling of isotope fractionation effects to improve quantification of biodegradation. Environ Sci Technol 42:2457–2463, doi:10.1021/es071981j

Van Breukelen BM, Rolle M (2012) Transverse hydrodynamic dispersion effects on isotope signals in groundwater chlorinated solvents' plumes. Environ Sci Technol 46:7700–7708, doi:10.1021/es301058z

VanCappellen P (1996) Reactive surface area control of the dissolution kinetics of biogenic silica in deep-sea sediments. Chem Geol 132:125–130, doi:10.1016/s0009-2541(96)00047-2

Verney-Carron A, Vigier N, Millot R (2011) Experimental determination of the role of diffusion on Li isotope fractionation during basaltic glass weathering. Geochim Cosmochim Acta 75:3452–3468, doi:10.1016/j.gca.2011.03.019

Vigier N, Bourdon B, Lewin E, Dupre B, Tuner S, Chakrapani GJ, van Calsteren P, Allegre CJ (2005) Mobility of U-series nuclides during basalt weathering: An example from the Deccan Traps (India). Chem Geol 219:69–91, doi:10.1016/j.chemgeo.2005.02.010

Vigier N, Decarreau A, Millot R, Carignan J, Petit S, France-Lanord C (2008) Quantifying Li isotope fractionation during smectite formation and implications for the Li cycle. Geochim Cosmochim Acta 72:780–792, doi:10.1016/j.gca.2007.11.011

Vigier N, Gislason SR, Burton KW, Millot R, Mokadem F (2009) The relationship between riverine lithium isotope composition and silicate weathering rates in Iceland. Earth Planet Sci Lett 287:434–441, doi:10.1016/j.epsl.2009.08.026

Wahl MH, Urey HC (1935) Vapour pressures of isotopic forms of water. J Chem Phys 3:411–414, doi:10.1063/1.1749690

Wanner C, Sonnenthal EL (2013) Assessing the control on the effective kinetic Cr isotope fractionation factor: A reactive transport modeling approach. Chem Geol 337:88–98, doi:10.1016/j.chemgeo.2012.11.008

Wanner C, Druhan JL, Amos RT, Alt-Epping P, Steefel CI (2014) Benchmarking the simulation of Cr isotope fractionation. Comput Geosci, doi:10.1007/s10596-014-9436-9

Watkins JM, Nielsen LC, Ryerson FJ, DePaolo DJ (2013) The influence of kinetics on the oxygen isotope composition of calcium carbonate. Earth Planet Sci Lett 375:349–360, doi:10.1016/j.epsl.2013.05.054

Watson EB (2004) A conceptual model for near-surface kinetic controls on the trace-element and stable isotope composition of abiogenic calcite crystals. Geochim Cosmochim Acta 68:1473–1488, doi:10.1016/j.gca.2003.10.003

Watson EB, Liang Y (1995) A simple model for sector zoning in slowly grown crystals: Implications for growth rate and lattice diffusion, with emphasis on accessory minerals in crustal rocks. Am Mineral 80:1179–1187

Weiss DJ, Boye K, Caldelas C, Fendorf S (2014) Zinc isotope fractionation during early dissolution of biotite granite. Soil Sci Soc Am J 78:171–179, doi:10.2136/sssaj2012.0426

White AF, Brantley SL (2003) The effect of time on the weathering of silicate minerals: why do weathering rates differ in the laboratory and field? Chem Geol 202:479–506, doi:10.1016/j.chemgeo.2003.03.001

Wiederhold JG (2015) Metal stable isotope signatures as tracers in environmental geochemistry. Environ Sci Technol 49:2606–2624, doi:10.1021/es504683e

Wiederhold JG, Kraemer SM, Teutsch N, Borer PM, Halliday AN, Kretzschmar R (2006) Iron isotope fractionation during proton-promoted, ligand-controlled, and reductive dissolution of goethite. Environ Sci Technol 40:3787–3793, doi:10.1021/es052228y

Williams LB, Hervig RL (2005) Lithium and boron isotopes in illite-smectite: The importance of crystal size. Geochim Cosmochim Acta 69:5705–5716, doi:10.1016/j.gca.2005.08.005

Wimpenny J, Gislason SR, James RH, Gannoun A, Pogge Von Strandmann PAE, Burton KW (2010) The behaviour of Li and Mg isotopes during primary phase dissolution and secondary mineral formation in basalt. Geochim Cosmochim Acta 74:5259–5279, doi:10.1016/j.gca.2010.06.028

Wolthers M, Nehrke G, Gustafsson JP, Van Cappellen P (2012) Calcite growth kinetics: Modeling the effect of solution stoichiometry. Geochim Cosmochim Acta 77:121–134, doi:10.1016/j.gca.2011.11.003

Wombacher F, Eisenhauer A, Boehm F, Gussone N, Regenberg M, Dullo WC, Rueggeberg A (2011) Magnesium stable isotope fractionation in marine biogenic calcite and aragonite. Geochim Cosmochim Acta 75:5797–5818, doi:10.1016/j.gca.2011.07.017

Worch E (1993) A new equation for the calculation of diffusion coefficients for dissolved substances. *In*: [Water]. Vol 81. Fachgruppe Wasserchemie in der Gesellschaft. C Deutscher (ed), p 289–297

Xu TF, Pruess K (2001) Modeling multiphase non-isothermal fluid flow and reactive geochemical transport in variably saturated fractured rocks: 1. Methodology. Am J Sci 301:16–33, doi:10.2475/ajs.301.1.16

Yamaguchi T, Matsuoka T, Koda S (2005) Generalized Langevin theory on the dynamics of simple fluids under external fields. J Chem Phys 123:03405, doi:10.1063/1.1955455

Yamaji K, Makita Y, Watanabe H, Sonoda A, Kanoh H, Hirotsu T, Ooi K (2001) Theoretical estimation of lithium isotopic reduced partition function ratio for lithium ions in aqueous solution. J Phys Chem A 105:602–613, doi:10.1021/jp001303i

Yoon H, Valocchi AJ, Werth CJ, Dewers T (2012) Pore-scale simulation of mixing-induced calcium carbonate precipitation and dissolution in a microfluidic pore network. Water Resour Res 48: W02524, doi:10.1029/2011wr011192

Yoon H, Kang Q, Valocchi A (2015) Lattice Boltzmann-based approaches for pore-scale reactive transport. Rev Mineral Geochem 80:393–431

Ziegler K, Chadwick OA, Brzezinski MA, Kelly EF (2005) Natural variations of delta Si-30 ratios during progressive basalt weathering, Hawaiian Islands. Geochim Cosmochim Acta 69:4597–4610, doi:10.1016/j.gca.2005.05.008